

Submitted to the Editor of the Astrophysical Journal
Revised April 22, 1997

Self-Consistent Fokker-Planck Treatment Of Particle Distributions in Astrophysical Plasmas

Sergei Nayakshin¹ and Fulvio Melia^{1,2,†}

¹*Department of Physics, University of Arizona, Tucson, AZ 85721*
[serg@physics.arizona.edu]

²*Department of Astronomy, University of Arizona, Tucson, AZ 85721*
[melia@as.arizona.edu]

† Presidential Young Investigator

ABSTRACT

High-energy, multi-component plasmas in which pair creation and annihilation, lepton-lepton scattering, lepton-proton scattering, and Comptonization all contribute to establishing the particle and photon distributions, are present in a broad range of compact astrophysical objects. The different constituents are often not in equilibrium with each other, and this mixture of interacting particles and radiation can produce substantial deviations from a Maxwellian profile for the lepton distributions. Earlier work has included much of the microphysics needed to account for electron-photon and electron-proton interactions, but little has been done to handle the redistribution of the particles as a result of their Coulomb interaction with themselves. The most detailed analysis thus far for finding the exact electron distribution appears to have been done within the framework of non-thermal models, where the electron distribution is approximated as a thermal one at low energy with a non-thermal tail at higher energy. Recent attention, however, has been focused on thermal models.

Our goal here is to use a Fokker-Planck approach in order to develop a fully self-consistent theory for the interaction of arbitrarily distributed particles and radiation to arrive at an accurate representation of the high-energy plasma in these sources. We conduct several tests representative of two dominant segments of parameter space. For high source compactness of the total radiation field, $l \sim 10^2$, we find that although the electron distribution deviates substantially from a Maxwellian, the resulting photon spectra are insensitive to the exact electron shape, in accordance with some earlier results. For low source compactness, $l \sim \text{few}$, and an optical depth $\lesssim 0.2$, however, we find that both the electron distribution and the photon spectra differ strongly from what they would be in the case of a Maxwellian distribution. In addition, for all values of compactness, we find that different electron distributions lead to different positron number densities and proton equilibrium temperatures. This means that the ratio of radiation pressure to proton pressure is strongly dependent on the lepton distribution, which might lead to different configurations of hydrostatic equilibrium. This, in turn, may change the compactness, optical depth, and heating and cooling rates, and therefore lead to an additional change in the spectrum. An important result of our analysis, is the derivation of useful, approximate analytical forms for the electron distribution in the case of strongly non-Maxwellian plasmas.

Subject headings: accretion disks—black hole physics—galaxies: Seyfert—gamma rays: theory—plasmas—radiative transfer

1. Introduction

There is a great deal of interest in the physics of relativistic, multi-component, astrophysical plasmas, which appear to be present in a wide variety of high-energy emitting objects, such as neutron stars, black holes, and Active Galactic Nuclei (AGNs). The particle distributions in these sources depend critically on key physical processes, such as pair creation and annihilation, lepton-lepton scattering, lepton-proton scattering, and Comptonization. Often, the particle population and the radiation field are not in equilibrium, and it is possible that in some cases, such as the inner coronal regions in black hole systems like Cygnus X-1 and 1E1740.7-2942, the electrons and protons are themselves not equilibrated, with the proton “temperature” greatly exceeding that of the electrons and positrons (Shapiro, Lightman & Eardley 1976; for a more recent discussion and more extensive list of references, see also Misra & Melia 1996).

The attention paid to these plasmas is fostered by continued, exciting observations of the underlying objects by a number of high-energy instruments on satellites such as the *Compton Gamma-Ray Observatory (CGRO)*. For example, OSSE and COMPTEL on *CGRO* have recently revealed that persistent MeV gamma-rays are emitted by several Galactic black hole candidates (GBHCs), including Cygnus X-1 (Johnson et al. 1993; McConnell et al. 1994) and GRO J0422+32 (van Dijk et al. 1995). Single component thermal models (e.g., Sunyaev & Titarchuk 1980; Titarchuk 1994) have difficulty accounting for these high-energy tails, which strongly hint at nonthermal processes. In these systems, not only is a substantial fraction of the radiation produced externally and therefore not initially in thermal equilibrium with the electron-positron pair plasma, but the combination of pair creation/annihilation (Liang 1979; Kusunose 1987; Svensson 1990; Melia & Misra 1993; Misra & Melia 1996), thermal and non-thermal radiation, and the heating of protons via gravitational energy dissipation, results in a mixture of interacting particles and radiation that produces important deviations from a Maxwellian profile for the lepton distribution. Recently, Li, Kusunose & Liang (1996) discussed a stochastic particle acceleration scheme to account for this high-energy emission, and concluded that the energized particles consist of a blend of thermal and nonthermal components. In addition, they found that for certain parameter regimes, acceleration is more efficient than the cooling processes and must therefore be taken into account when determining the particle distributions of the emitting plasma. Most importantly, they showed that a deviation of the particle distribution from a Maxwellian at high energies can account for most of the emission above 1 MeV via inverse-Compton scattering.

This alone makes the fully-consistent approach we describe here essential for a more complete understanding of the high-energy emission in GBHCs, but there are several equally important additional aspects to this problem. One of these is the appearance of a transient \sim MeV bump discovered in Cygnus X-1 by Ling et al. (1987), which is difficult to explain with the preliminary study of Li et al. (1996). Earlier, Melia & Misra (1993) suggested that the transient bump might be due to bremsstrahlung-self-Compton processes within the gravitationally-compressed, inner hot region of the disk. However, without a complete analysis of the actual particle distribution, including its deviations at high energy, this hypothesis remains to be tested. A second important concern is the rapid spectral variability in these sources, which the *Rossi X-Ray Timing Explorer* is now beginning to sample with sub-millisecond resolution. Since the rapid acceleration and cooling

processes affect the particle energy re-distribution on this time scale (e.g., Melia & Misra 1993), it would be highly desirable to have a time-dependent scheme to track the particle and spectral evolution in a self-consistent manner. The approach described in this paper will be able to address each of these issues.

The OSSE instrument on *CGRO* has also detected several Seyfert galaxies above 60 keV (e.g., Maisack et al. 1993; Cameron et al. 1995; Madejski 1995), showing a break or an exponential cut-off at $\sim 50 - 100$ keV, with an overall spectrum not unlike those of the GBHCs (e.g., Sunyaev et al. 1991). Together with X-ray observations by GINGA, these OSSE data suggest that a single robust mechanism may be operating in both classes of sources (Fabian 1994). However, although basic models such as the pure non-thermal pair model (for a review, see Svensson 1994) predict a steepening of the hard X-ray spectrum, they do not easily produce a break as sharp as that seen by OSSE. In addition, they predict a flattening of the spectrum at $\sim 100 - 200$ keV, and an annihilation line, neither of which has been observed so far. The Seyfert spectra may instead be based on thermal models, or more realistically, quasi-thermal models (e.g., Haardt & Maraschi 1991, 1993; Ghisellini, Haardt & Fabian 1993; Titarchuck & Mastichiadis 1994; Zdziarski et al. 1994; Zdziarski et al. 1995; Haardt, Maraschi & Ghisellini 1996; see Svensson 1996 for a recent review). In the past, purely thermal models for the high-energy spectra of AGNs have been criticized on the basis of the long thermalization time needed to attain thermal equilibrium at high temperatures. The reason for this is that the observed X-ray variability time scale is shorter than the inferred time required for two-body thermalization, suggesting that the plasma cannot be Maxwellian. Thus, both thermal and non-thermal models for the X-ray spectra in Seyfert galaxies have significant problems. In some regions of parameter space, non-thermal and thermal particle distributions produce very similar spectra, as long as the radiative process is multi-Compton scattering and the maximum particle energy is a few MeV (Ghisellini et al. 1993), suggesting that a compromise model may still work. However, this similarity in spectra occurs only for a restricted range of optical depths and source photon compactness, and the assumed dynamics of the emitting plasma may not be consistent with the luminosities implied by the observed photon emissivities. There is clearly a need to establish the correct (non-Maxwellian) particle distribution in these sources for a broad range of system parameters. In a portion of the available phase space, the photons are not multiply-scattered so the resultant spectrum will in fact reflect the underlying particle distribution. Very importantly, the self-consistently determined particle and photon populations must be reconciled with the permitted system-dependent considerations, such as the allowed compactness and lepton temperature, which turn out to be dependent upon the actual electron and positron distributions for part of the parameter space.

Our goal in this paper is to begin the process of developing a fully self-consistent theory for the interaction of arbitrarily distributed particles and radiation to arrive at an accurate representation of the high-energy plasma in compact sources. We first consider the non-Maxwellian parameter space in §2. We then motivate the use of the Fokker-Planck approach in §3, and we derive the general Fokker-Planck coefficients for arbitrary particle distributions in §4. In §5 we extend the generality of our scheme by including the electron/positron-proton interaction and the effects due to Comptonization (pair creation and annihilation are included by means of some standard formulae available in the literature and discussed in §6). We test the algorithm in §6. Much attention in that

section is paid to the physical consequences of the distribution function being non-Maxwellian. We end with our conclusions in §7. The Appendix describes in detail the numerical time-dependent scheme that has been used to solve the full electron-photon-proton set of equations. The reasons for neglecting large angle scatterings in the diffusion coefficient are also given in the Appendix.

2. The Non-Maxwellian Parameter Space

In this section, we discuss briefly the circumstances under which one should reasonably expect to see the electron distribution deviating substantially from a Maxwellian shape. Although this issue is covered extensively in the literature (e.g., Stepney 1983; Guilbert and Stepney 1985; DL89; Baring 1987; Ghisellini, Haardt & Fabian 1993, hereafter GHF; Fabian 1994), there seems to be no simple expression which would characterize the parameter space where the non-thermal distribution can form for a general source geometry and arbitrary optical depth. Our goal here is to provide such an expression.

The most likely process to dominate the truncation of the electron distribution is inverse Compton cooling on low energy photons (Fabian 1994). As is well known (e.g., Rybicki & Lightman 1979), the rate of energy transfer in the Thomson scattering regime, from a single electron with gamma-factor γ to soft photons with energy density U_{ph} , is

$$m_e c^2 \left(\frac{dE}{dt} \right)^- = \frac{4}{3} \sigma_T c \beta^2 \gamma^2 U_{\text{ph}} , \quad (1)$$

where U_{ph} is the soft photon energy density within the source. For a source with a spherical geometry of radius R , one can approximate this expression as

$$\left(\frac{dE}{dt} \right)^- \simeq (4/3) l (\beta \gamma)^2 \frac{c(1 + \tau_T)}{R} , \quad (2)$$

where $l \equiv L\sigma_T/4\pi R m_e c^3$ is the compactness of the region, and L is the total source luminosity. Equation (2) does not change for a disk geometry, but the compactness l should then be replaced by $l = L\sigma_T/hm_e c^3$, where h is the geometrical thickness of the disk, and L is the luminosity of a cube h^3 (i.e., the standard definition of l ; e.g., Svensson 1996; § 6).

For the electron-electron energy exchange rate, we will use an approximation that is well known in the literature and re-derived below (Eq. 30). This approximation is valid for $E (\gg \Theta_e)$ equal to the average thermal γ -factor $\langle \gamma \rangle$:

$$\left(\frac{dE}{dt} \right)_{\text{ee}} \simeq -(3/2) \frac{\ln \Lambda}{t_T} \frac{1}{\beta \langle \gamma \rangle} . \quad (3)$$

Let us now introduce the parameter λ which will give the ratio of the inverse Compton cooling rate to the e-e Coulomb energy transfer rate for the average electron:

$$\lambda \equiv \frac{|\left(\frac{dE}{dt} \right)^-|}{|\left(\frac{dE}{dt} \right)_{\text{ee}}|} \simeq \left(\frac{l(1 + \tau_T)}{\tau_T \ln \Lambda} \right) \langle \beta \gamma \rangle^3 , \quad (4)$$

where $\tau_T \equiv n_e \sigma_T R$ is the Thomson optical depth. Considering the relativistic and non-relativistic limits of $\langle \beta \gamma \rangle^3$, and merging these two expressions for the mildly relativistic domain, one can simplify Equation (4) to

$$\lambda \simeq \frac{l(1 + \tau_T)}{\tau_T \ln \Lambda} \left(\frac{3}{2} \Theta_e \right)^{3/2} \left[1 + (6 \Theta_e)^{3/2} \right] . \quad (5)$$

The physical significance of this parameter is such that when λ is of order unity, one should expect a noticeable truncation in the tail of the Maxwellian distribution. It is *not* a quantitative parameter that describes exactly how the high energy tail of the Maxwellian is truncated, because this is determined not only by electron-photon and electron-electron interactions, but also by the interaction that heats the electrons. Note that $\lambda \gtrsim 1$ does not necessarily mean that the photon spectrum will be changed significantly due to such a truncation (see the tests in § 6 below).

One can rewrite Equation (5) in terms of the maximum compactness of the region where e-e Coulomb collisions can still maintain a Maxwellian distribution. This gives an expression similar to the one derived by Fabian (1994), except for the factor $(1 + \tau_T)/\tau_T$, which was approximated by unity for $\tau_T \gtrsim 1$. Since recently much attention has been given to optically thin plasmas (e.g., Svensson 1996), we will here retain this factor.

Another competitive thermalization process is the so called synchrotron boiler (e.g., Ghisellini, Guilbert & Svensson 1988). It turns out that synchrotron photons emitted and re-absorbed by electrons can be a very important mechanism for the electron thermalization. Although we do not consider this thermalization mechanism in this paper, i.e., we assume that magnetic field is small, it is necessary to assess the importance of this process. The total synchrotron power emitted by an electron is given by an equation similar to Equation (1), except that the radiation energy density should be replaced by the magnetic field energy density ($U_{\text{mag}} = B^2/8\pi$). Thus, when the magnetic field energy density is larger than the radiation energy density, the electron distribution will be thermalized due to the synchrotron self-absorption process or due to Coulomb electron-electron interactions, if the latter dominate. To see when synchrotron thermalization dominates over Coulomb thermalization, let us define a ‘magnetic’ thermalization parameter, λ_m . Following Ghisellini, Guilbert & Svensson (1988), we first define the magnetic compactness parameter l_b :

$$l_b \equiv U_{\text{mag}} \frac{R\sigma_T}{m_e c^2}. \quad (6)$$

The synchrotron self-absorption will dominate as a thermalizing mechanism if λ_m , defined as the ratio of the synchrotron emissivity to the electron-electron energy exchange rate, is larger than unity:

$$\lambda_m \simeq \frac{l_b}{\tau_T \ln \Lambda} \left(\frac{3}{2} \Theta_e \right)^{3/2} \left[1 + (6 \Theta_e)^{3/2} \right] \gtrsim 1. \quad (7)$$

Here we have followed the same steps as those leading to Equation (5). The physical significance of λ_m is that if it larger than unity, then synchrotron self-absorption thermalization dominates over Coulomb thermalization. It is interesting to note that recent models for the origin of X-rays in Seyfert Galaxies invoke short-lived and intense magnetic flares on the surface of a cold accretion disk (e.g., Haardt, Ghisellini & Maraschi 1994; Nayakshin & Melia 1997a). In these flares $l_b > l$, since the conditions for plasma confinement require that radiation pressure (the dominant pressure in the case $l \gg 1$) is much smaller than the magnetic stress (Nayakshin & Melia 1997b). Therefore, it is very likely that the synchrotron processes keeps the particles thermal in such flares, unless the heating mechanism acts in the opposite direction (the heating mechanism is likely to be of a collective rather than a two-body nature, and it is still unknown; see § 6 below). In other circumstances, e.g., inside of the accretion disk, the magnetic field energy density must

certainly be below the equipartition value, and for the radiation dominated part of the disk, the ‘synchrotron thermalization’ will be weaker than inverse Compton cooling. For our purposes here, we restrict the parameter space of interest to the regions where λ_m is smaller than 1, so that Coulomb thermalization dominates.

We should also note that other processes are unlikely to be of a real importance in determining the shape of the equilibrium electron distribution (this will be clear from the discussion below). For example, pair creation and annihilation is a considerably slower process; we experimented with non-thermal models where pairs are injected with some power-law distribution (e.g., Lightman & Zdziarski 1987), and found that pairs have essentially the same distribution as the electrons everywhere, except that normalization of the power-law component is different with respect to the thermalized part of the distribution. Thus, it is fair to assume that the electrons and positrons have the same distributions but with different normalizations. Next, proton heating is also unlikely to change the shape of the electron distribution because it is strongest at the low energy end. In that region, the equilibrium distribution when only the proton-electron interactions remain in the full equation is a Maxwellian with the proton temperature. But for the low energy end ($E \ll kT$), the electron distribution function is the same for all temperatures, differing only by its normalization. Therefore, the low energy end of the electron distribution function in the presence of proton heating has the Maxwellian shape, irrespective of how strong the proton heating is. If the electron heating mechanism is different from proton heating, however, then there is a possibility that it will lead to deviations from a Maxwellian on the low energy end (where it is the strongest, presumably), but we leave this for future work since the exact heating mechanism is not yet known.

3. The Fokker-Planck Approximation For Coulomb Interactions

As is well known, the Coulomb cross-section diverges for small angle scattering, where the relative change in the particle’s energy approaches a negligible value (e.g., Chandrasekhar 1942). It is therefore unwise and numerically very challenging to treat Coulomb scattering using the otherwise commonly employed Boltzmann collision integral. Instead, this feature of the Coulomb force lends itself more naturally to a Fokker-Planck (FP) approach for solving the kinetic equation in the presence of an r^{-2} type of interaction. The FP procedure is particularly powerful when the change in particle energy ΔE is much smaller than its incident energy E . When this holds, the distribution functions appearing inside the Boltzmann collision integral can be decomposed as power series in the small expansion parameter $\Delta E/E$ ($\ll 1$). An example of how this works in practice is the Kompaneets equation (Kompaneets 1957), which is well-known in astrophysics.

When the particle distribution function is isotropic and homogeneous in space, the FP equation for the distribution function takes the form

$$\frac{\partial f(E, t)}{\partial t} = -\frac{\partial}{\partial E} \left[a(E, t) f(E, t) \right] + \frac{1}{2} \frac{\partial^2}{\partial E^2} \left[D(E, t) f(E, t) \right], \quad (8)$$

where $f(E, t)$ is the distribution function of electrons in energy space (i.e., $f(E, t) = \beta \gamma^2 f^*(E, t)$, E is kinetic energy of the electron in units of $m_e c^2$, $E = (\gamma - 1)$, $\beta \equiv (1 - 1/\gamma^2)^{1/2}$ and $f(E, t) dE \equiv f^*(\vec{p}, t) d^3 \vec{p}$ gives the volume density of electrons in the phase space element $d^3 \vec{p}$, and \vec{p} is the electron momentum in units $m_e c^2$), $a(E, t)$ is the average energy exchange rate and $D(E, t)$ is the

energy dispersion rate of the test particle. Both $a(E, t)$ and $D(E, t)$ are functions of time because the distribution function over which they are convolved depends on time. Since E is dimensionless, we will use E and $(\gamma - 1)$ interchangeably throughout the paper, and $f(\gamma)$ is the same distribution as $f(E)$.

In their application of this equation to the study of electron thermalization in a background relativistic Maxwell-Boltzmann (MB) plasma, Dermer and Liang (1989) derived the FP coefficients for a small population of particles scattering off a relativistic MB distribution. In this limit where the test particle number density is much lower than that of the background MB plasma, Equation (8) is linear in the distribution function $f(E, t)$. However, this approach fails when the real electron distribution differs substantially from the perfect (background) MB profile. The original motivation for taking this simplified approach was to produce one-dimensional integrals for the FP coefficients. However, as we shall see in §4 below, the FP coefficients derived there for an arbitrary particle distribution are themselves simply one-dimensional integrals and there is therefore no computational advantage to be had in restricting the problem to the quasi-thermalized initial condition if the temperature is allowed to evolve. Of course, our generalized approach is practical only if we can find a numerical scheme that makes the problem tractable. The nature of the computational scheme that solves this problem is discussed in detail in the Appendix.

4. Coulomb Electron-Electron Fokker-Planck Coefficients For Arbitrary Particle Distributions

4.1. The Single Particle Energy Exchange $a(\gamma, \gamma_1)$ and Diffusion $D(\gamma, \gamma_1)$ Coefficients

We begin by deriving the Fokker-Planck coefficients for e-e Coulomb interactions for a mono-energetic particle distribution. The FP coefficients for an arbitrary particle profile can be calculated from these by convolving them over $f(E, t)$. We consider the FP energy exchange and diffusion coefficients for a test particle with dimensionless energy $E \equiv (\gamma - 1)$ (all electron energies are in units of $m_e c^2$ in this paper) Coulomb scattering off a mono-energetic electron (positron) distribution with energy $E_1 \equiv (\gamma_1 - 1)$. Our notation and some of our starting equations are based on earlier work by Dermer (1985) and Dermer & Liang (1989) (DL89 hereafter).

The distribution function is normalized by the condition

$$1 = \int_1^{\infty} d\gamma \beta \gamma^2 f^*(\gamma) \equiv \int_1^{\infty} d\gamma f(\gamma) . \quad (9)$$

For two such functions $f_1^*(\gamma_1)$ and $f_2^*(\gamma_2)$, the relativistically correct reaction rate is

$$r = \frac{cn_1 n_2}{2(1 + \delta_{12})} \int_1^{\infty} d\gamma_r (\gamma_r^2 - 1) \int_1^{\infty} d\gamma_c (\gamma_c^2 - 1)^{1/2} \int_{-1}^1 du f_1^*(\gamma_1) f^*(\gamma_2) \sigma(\gamma_r, \gamma_c) , \quad (10)$$

where n_1 and n_2 are the corresponding particle number densities, γ_r is the invariant relative Lorentz factor and γ_c is the Lorentz factor associated with velocity of the center of momentum (CM) frame relative to the lab frame (Dermer 1984, 1985). Here, $u \equiv \cos \mu$, and the variable μ is defined as the angle between the velocity of the CM frame and the particle 1 velocity in that frame. The Kronecker delta δ_{12} prevents double counting.

To arrive at the relativistically correct reaction rate for two mono-energetic distributions, we take the particle functions $f_i^*(\gamma_i)$, $i = 1, 2$, to be

$$f_i^*(\gamma_i) = \frac{1}{\beta_i \gamma_i^2} \delta(\gamma'_i - \gamma_i) , \quad (11)$$

where $\beta_i \equiv (1 - 1/\gamma_i^2)^{1/2}$, γ'_i are the laboratory frame Lorentz factors of the colliding particles expressed in terms of the relative Lorentz factor γ_r , and the CM Lorentz factor γ_c :

$$m_{1(2)} \gamma'_{1(2)} = \frac{\gamma_c}{S^{1/2}} \left[(m_{2(1)} \gamma_r + m_{1(2)}) \pm \beta_c m_{2(1)} \beta_r \gamma_r u \right] , \quad (12)$$

where $S \equiv m_1^2 + m_2^2 + 2m_1 m_2 \gamma_r$ and $+$ is for $i = 1$, while $-$ sign is for $i = 2$.

In deriving the energy exchange coefficient, we use inside the integral of Equation (10) the energy exchange rate $\langle \sigma(\gamma_r, \gamma_c) \Delta E \rangle$ for Coulomb interactions averaged over all *small* (see below) scattering angles in the center of momentum frame given explicitly by

$$\langle \sigma(\gamma_r, \gamma_c) \Delta E \rangle = \int d^3 \vec{p}^* \frac{d\sigma}{d\vec{p}^{*3}} \Delta E(\vec{p}^*) , \quad (13)$$

where ΔE is the energy exchange per scattering (in the laboratory frame) and \vec{p}^* is the particle momentum in the center of momentum frame.

Before we proceed with the derivation, we note that it only makes sense to talk about FP coefficients for the Coulomb interactions for small scattering angles. Even though such interactions dominate in the Coulomb scattering cross section, one must explicitly exclude the large scattering angles in the integrals for the FP coefficients. We will show later that inclusion of these angles in the FP coefficients (as done by DL89, for example) leads to erroneous results. Instead, the large angle scatterings must be included by means of the exact Boltzmann equation, that is the original integral equation from which the FP equation is derived. Following the standard practice, we neglect the large scattering angles in the Coulomb interactions in this paper.

Using the notation of Dermer (1984, 1985), the change in electron energy is

$$\Delta E = \gamma_c \beta_c p^* \left[(\cos \Psi^* - 1) \cos \mu - \sin \Psi^* \cos \phi^* \sin \mu \right], \quad (14)$$

where Ψ^* is the scattering angle in the center of momentum system, and ϕ^* is the polar angle in the C-system of coordinates (i.e., the CM frame in which the z -axis is directed along the unscattered particle 1 momentum; see Dermer 1985, Fig.1). Because the CM frame Lorentz γ -factor γ^* of the colliding electrons is $\gamma^* = \sqrt{(\gamma_r + 1)/2}$ for particles of equal mass, and $p^* = \beta^* \gamma^*$, the integration in Equation (13) is only carried out over angles ϕ^* from 0 to 2π and Ψ^* from Ψ_{\min}^* to some Ψ_{\max}^* (see below).

Since we limit ourselves to the small scattering angles, $\Psi^* \ll 1$, we can leave only the leading terms in the Coulomb scattering cross section, which is then equal to

$$\frac{d\sigma}{d \cos \Psi^*} = \frac{2\pi r_e^2 (2\gamma^{*2} - 1)^2}{\gamma^{*2} (\gamma^{*2} - 1)^2} \frac{1}{(1 - \cos^2 \Psi^*)^2} \quad (15)$$

(see, e.g., Jauch & Rohrlich 1980), where r_e is the classical electron radius.

The exact value of Ψ_{\max}^* is usually considered to be unimportant and therefore often chosen as $\pi/2$ for simplicity (e.g., Landau and Lifshitz 1981; Dermer 1985). Because the second term inside the brackets in Equation (14) gives zero after averaging over ϕ^* , the energy exchange rate in the CM frame is then

$$\langle \sigma(\gamma_r, \gamma_c) \Delta E \rangle = \int_{\cos \Psi_{\min}^*}^{\cos \Psi_{\max}^*} d \cos \Psi^* \frac{d\sigma}{d \cos \Psi^*} \gamma_c \beta_c p^* \left[(\cos \Psi^* - 1) \cos \mu \right]. \quad (16)$$

Taking the integral and expressing p^* in terms of γ_c and γ_r , we obtain

$$\langle \sigma(\gamma_r, \gamma_c) \Delta E \rangle = 8 \pi r_e^2 \ln \Lambda \frac{\gamma_r^2 \gamma_c \beta_c}{\sqrt{2(\gamma_r + 1)(\gamma_r - 1)^3}} u, \quad (17)$$

where $\ln \Lambda \equiv \ln \left[(1 - \cos \Psi_{\max}^*) / (1 - \cos \Psi_{\min}^*) \right]^{1/2}$ is the Coulomb logarithm. We set $\ln \Lambda = 20$ throughout the paper.

From Equation (10), we now infer the general expression for the energy exchange coefficient (note that this expression is now for a single electron, so n_2 no longer enters the expression; also

the factor with the Kronecker δ_{12} was discarded since we now are interested in the energy exchange rate for a given particle rather than the total interaction rate):

$$a(\gamma, \gamma_1) = \frac{cn_1}{2\beta\gamma^2\beta_1\gamma_1^2} \int_1^\infty d\gamma_r (\gamma_r^2 - 1) \int_1^\infty d\gamma_c (\gamma_c^2 - 1)^{1/2} \int_{-1}^1 du \delta\{\gamma - \gamma'_2\} \delta\{\gamma_1 - \gamma'_1\} \langle \sigma(\gamma_r, \gamma_c) \Delta E \rangle. \quad (18)$$

Performing the third integration first, one finds

$$\int_{-1}^1 du \delta\{\gamma - \gamma'_2\} \langle \sigma(\gamma_r, \gamma_c) \Delta E \rangle = -\frac{8\pi r_e^2 \ln \Lambda}{m_e^2} \frac{S\gamma_r^2 \sqrt{(\gamma_r - 1)/2}}{(\gamma_r^2 - 1)^2 (\gamma_r - 1) \gamma_c \beta_c} \left(\gamma - \gamma_c \frac{\gamma_r + 1}{(S^{1/2}/m_e)} \right), \quad (19)$$

subject to the condition that $|\cos \mu| \equiv |u| \leq 1$, which leads to the constraint

$$\frac{(S^{1/2}/m_e)}{\gamma_r \beta_r \gamma_c \beta_c} \left| \gamma - \gamma_c \frac{\gamma_r + 1}{(S^{1/2}/m_e)} \right| \leq 1. \quad (20)$$

According to Equation (12), γ_c is fixed by the expression $\gamma_c = (\gamma + \gamma_1)/(S^{1/2}/m_e)$ when $m_1 = m_2 = m_e$. Equation (20) then leads to a restriction on the range of physically accessible values of γ_r in the integral of Equation (18), which we write as $\gamma^- \leq \gamma_r \leq \gamma^+$, where $\gamma^\pm = \gamma_1 \gamma (1 \pm \beta_1 \beta)$.

The next step is to compute the integral over γ_c :

$$\int_1^\infty d\gamma_c \gamma_c \beta_c \int_{-1}^1 du \delta\{\gamma - \gamma'_2\} \delta\{\gamma_1 - \gamma'_1\} \langle \sigma(\gamma_r, \gamma_c) \Delta E \rangle = -\frac{4\pi r_e^2 \ln \Lambda}{(\gamma_r^2 - 1)^{3/2} (\gamma_r - 1)} (\gamma - \gamma_1). \quad (21)$$

The final integral leads to the energy exchange coefficient, which we write as

$$a(\gamma, \gamma_1) = -\frac{2\pi r_e^2 cn_1 \ln \Lambda}{\beta_1 \gamma_1^2 \beta \gamma^2} (\gamma - \gamma_1) \chi(\gamma, \gamma_1), \quad (22)$$

where $\chi(\gamma, \gamma_1)$ is the integral function defined by

$$\chi(\gamma, \gamma_1) = \int_{\gamma^-}^{\gamma^+} dx \frac{x^2}{\sqrt{(x+1)(x-1)^3}}. \quad (23)$$

This integration can be carried out analytically, giving

$$\chi(\gamma, \gamma_1) = \left[-\sqrt{\frac{x+1}{x-1}} + 2 \sinh^{-1} \left(\sqrt{\frac{x-1}{2}} \right) + \sqrt{x^2 - 1} \right]_{\gamma^-}^{\gamma^+}. \quad (24)$$

Note that since γ^\pm is symmetric in γ and γ_1 , the energy exchange rate given by Eq.(22) is antisymmetric with respect to the interchange $\gamma \leftrightarrow \gamma_1$.

For the diffusion coefficient, we proceed in a similar fashion. Now, however, it is imperative (see Appendix A.4) that we choose $\Psi_{\max}^* \ll 1$. We square Equation (14) and consider the term with

$(1 - \cos \Psi^*)^2$. If one takes $\Psi_{\max}^* = \pi/2$, angles $\Psi^* \sim 1$ will dominate the contribution of this term to the integral over Ψ^* . But this is the parameter space where the FP equation becomes invalid, thus we cannot simply suggest $\Psi_{\max}^* = \pi/2$ and must use $\Psi_{\max}^* \ll 1$. In that case, contribution of the first term in Equation (14) is negligible compared to the second term in the brackets. Accordingly,

$$\langle \sigma(\gamma_r, \gamma_c) (\Delta E)^2 \rangle = \frac{4\pi r_e^2 \gamma_r^2 (\gamma_c^2 - 1)}{\gamma_r^2 - 1} \ln \Lambda (1 - u^2), \quad (25)$$

and after carrying out the necessary integrations, we arrive at

$$D(\gamma, \gamma_1) = \frac{4\pi r_e^2 c n_1 \ln \Lambda}{\beta_1 \gamma_1^2 \beta \gamma^2} \left[\frac{1}{2} (\gamma - \gamma_1)^2 \chi(\gamma, \gamma_1) + \zeta(\gamma, \gamma_1) \right]. \quad (26)$$

The function $\zeta(\gamma, \gamma_1)$ is defined as

$$\zeta(\gamma, \gamma_1) = \int_{\gamma^-}^{\gamma^+} dx \frac{x^2}{\sqrt{x^2 - 1}} \left[\frac{(\gamma + \gamma_1)^2}{2(1+x)} - 1 \right]. \quad (27)$$

The integrand is a relatively well behaved function, and the integral is easy to evaluate numerically as well as analytically.

Figures 1 and 2 show the FP energy exchange $a(\gamma, \gamma_1)$ and dispersion $D(\gamma, \gamma_1)$ coefficients, respectively, as functions of γ for three different values of γ_1 . In these figures, t_C is the Thomson time divided by the Coulomb logarithm ($t_C \equiv 1/n_e c \sigma_T \ln \Lambda$). It is evident that $a(\gamma, \gamma_1)$ is a discontinuous function of γ ; at $\gamma = \gamma_1$ it changes sign from a non-zero positive value to a non-zero negative one. This non-physical behavior is caused by the divergence of the original Coulomb scattering cross section for $|\vec{v}_1 - \vec{v}_2| \ll v_1$. This discontinuity in $a(\gamma, \gamma_1)$ for $|\vec{v}_1 - \vec{v}_2| \ll v_1$ is not a problem physically, because the parameter space for such interactions is very small and will contribute negligible to the electron-electron Coulomb interactions. It is also never a problem numerically. The convolution of $a(\gamma, \gamma_1)$ over any real physical distribution (i.e., a reasonably smooth one) smoothes out this non-physical behavior and practically eliminates the problem (one can show that electrons with energies $|\gamma_1 - \gamma| = \Delta E$ have $a(\gamma, \gamma_1) \propto (\Delta E)^2$ for any continuous $f(\gamma)$).

A well known fact is seen from Figure 1: particles with lower energy both gain and lose energy (depending on how energetic their interacting partners are) faster than the more energetic ones. This happens because of the dependence of the Coulomb scattering cross section on energy of the colliding particles in the CM frame (Eq. 14).

It is possible to derive analytical limits for the FP coefficients. For $\beta_1 \ll 1$ one gets from Equation (22) the limiting form for $a(\gamma, \gamma_1)$:

$$a(\gamma, \gamma_1) = \begin{cases} (3/2) 1/t_C \beta_1, & \text{for } \gamma < \gamma_1 \\ -(3/2) 1/t_C \beta, & \text{for } \gamma > \gamma_1 \end{cases}. \quad (28)$$

In the limit $\gamma \gg \gamma_1 \gg 1$ it is also possible to have an analytic approximation for $a(\gamma, \gamma_1)$:

$$a(\gamma, \gamma_1) \simeq -(3/2) \frac{1}{t_C} \left(\frac{1}{\gamma_1} - \frac{1}{\gamma} \right) \simeq -(3/2) \frac{1}{t_C} \frac{1}{\gamma_1}. \quad (29)$$

We can merge these two expressions in the case of $E \equiv \gamma - 1 \gg E_1 \equiv \gamma_1 - 1$ to give

$$a(\gamma, \gamma_1) = - (3/2) \frac{1}{t_C} \frac{1}{\beta \gamma_1} \quad (30)$$

4.2. FP Coefficients For Arbitrary Particle Distributions: Examples

Now that we have the mono-energetic coefficients in hand, finding those for any given arbitrary particle distribution $f(\gamma_1)$ is simply a matter of convolving these with the particle profile:

$$a(\gamma) = \int d\gamma_1 f(\gamma_1) a(\gamma, \gamma_1), \quad (31)$$

and similarly for $D(\gamma)$.

To illustrate how this works in practice, we show in Figures 3 and 4 the e-e Coulomb energy exchange and diffusion coefficients for three different distributions: (1) a perfect Maxwellian at temperature $\Theta_e = 1$, (2) a Gaussian with the same average energy, and (3) a power-law $f(\gamma) = \beta \gamma^{-p}$ (with the maximum $\gamma_{\max} - 1 = 100$, $\gamma_{\min} - 1 = 0.007$ and $p = 2.48$). The power-law and the Gaussian are chosen as two opposite representative cases, the former broader than and the latter narrower than the Maxwellian. All three distributions are normalized to unity and are plotted in Figure 5.

We note that the zeros of the energy exchange coefficient occur not at $\gamma = \langle \gamma_1 \rangle$, where $\langle \gamma_1 \rangle$ is the average Lorentz factor of the distribution, but rather at the maximum of the number distribution function. It is evident also that the quantity $\int d\gamma |a(\gamma)|$ is larger for the more diffuse distributions. The diffusion coefficient behaves in the opposite way. The larger diffusion coefficient corresponds to the sharper distribution function. Summarizing, we conclude that if the distribution is broader than a Maxwellian, it will be brought to the thermal distribution by the energy exchange coefficient, whereas if it is narrower, it will reach the thermal distribution as a result of the diffusion coefficient.

Dermer and Liang (1989) derived the energy exchange and the diffusion coefficients for the Coulomb interactions of a test electron with a background Maxwell-Boltzmann electron plasma. For the Maxwellian distribution, our results for the energy exchange coefficient are in complete agreement (to $1/\ln \Lambda$ precision) with those of DL89. For the diffusion coefficient, however, our expression disagrees with theirs at both the high and low energy end. Comparing the two expressions (Boettcher, 1996, private communication) one finds that they agree with each other well in the region $E \sim \Theta_e$ (up to the same precision of $1/\ln \Lambda$), but seriously disagree for $E \ll \Theta_e$ and $E \gg \Theta_e$. We find that $D(\gamma, \Theta_e) \simeq \text{const} (\approx 2\Theta_e |a(\infty, \Theta_e)|)$ for $E \gg 3\Theta_e$, while DL89 found that $D(\gamma, \Theta_e) \simeq \text{const}' \times E$ in that limit. We also find $D(\gamma, \Theta_e) \propto \beta^{1/2}$ on the low energy end, whereas DL89 found $D(\gamma, \Theta_e) \propto \text{const}$. The difference results from the fact that DL89 used $\Psi_{\max}^* = \pi/2$, and also left the terms leading to large scattering angles in the Coulomb cross section (see Appendix A.4) Taking into account the fact that $a(\gamma, \Theta_e) \simeq -\text{const}$ for $E \gg 3\Theta_e$, we see from Equation (8) that the equilibrium Maxwellian distribution can be reached only for $D(\gamma, \Theta_e) \simeq \text{const}$ at the high energy end. If instead, $D(\gamma, \Theta_e) \simeq \text{const}' \times E$ were the correct behavior, then one would find that the equilibrium $f(\gamma)$ is a power-law in the high energy limit. Since the original Boltzmann collision integral for Coulomb interactions leads to a Maxwellian electron distribution, this property must be preserved by the FP equation.

4.3 The Thermalization Process and Time Scales

An interesting question to consider is the following: Is self-consistent thermalization faster or slower than the thermalization of a test particle distribution interacting with a (fixed) background Maxwell-Boltzmann plasma? The answer is not obvious because both of the FP coefficients play a role in establishing the Maxwellian distribution, and as we saw in the previous section, if a distribution’s energy exchange coefficient is larger than that of the Maxwellian, the diffusion coefficient is smaller, and vice versa.

To answer this question, at least illustratively, we consider the thermalization of a Gaussian electron distribution in two special cases: (a) when the electrons interact with each other (i.e., solving the fully non-linear problem), and (b) when they thermalize on a background MB gas with the same average energy as that of the Gaussian distribution. In order to characterize the interaction quantitatively, we define the thermalization time scale t_r to be the time it takes the particle population to reach a deviation of 5% or less from a perfect Maxwellian, where the deviation ε is defined to be

$$\varepsilon \equiv \frac{\int_1^{\infty} d\gamma (\gamma - 1) |f(\gamma, t) - f_M(\gamma)|}{\int_1^{\infty} d\gamma (\gamma - 1) f_M(\gamma)} . \quad (32)$$

In this expression, $f(\gamma, t)$ and $f_M(\gamma)$ are, respectively, the actual time-dependent distribution function and the perfect Maxwellian with the same average energy and number of particles.

Our tests indicate that to within $\sim 5\%$ accuracy, the time scale for the test particle thermalization coincides with that for the self-interacting case. The explanation for this appears to be that most of the elapsed time occurs during the period when the distribution is close to Maxwellian, when in fact the FP coefficients for the time-dependent distribution and those for the Maxwellian are very similar. As such, our results are in very good agreement with the findings of DL89:

$$t_r = 4t_T \Theta_e^{3/2} (\pi^{1/2} - 1.2\Theta_e^{1/4} + 2\Theta_e^{1/2}) / \ln \Lambda , \quad (33)$$

where $t_T = (n_1 c \sigma_T)^{-1}$ is the Thomson time. At the same time we find that the thermalization time depends on the shape of the initial distribution. However, if one keeps the shape of the initial distribution fixed (e.g., a power-law) and observes the temperature dependence of the thermalization time, it is practically identical to Equation (33).

Figures 6 and 7 show the time evolution of the initial distribution functions, a power-law and a Gaussian, respectively, as they approach the equilibrium Maxwellian. The equilibrium temperature is the same for both distributions and equals $0.3 m_e c^2$. Figure 8 shows the time dependence of the deviation ε for both cases. It is notable that thermalization of the Gaussian happens much faster than that of the power-law. (When comparing the figures for these two cases, one should bear in mind the fact that different parts of the distribution function contribute to the integral in Eq. (32) with different weights, namely, E^2 . Thus, the high energy end of the electron distribution contributes much more to the deviation ε than the low energy end.) To explain this fact, we should consider the Coulomb interaction time scale for individual particles. Let us define the

particle energy time scale t_e as

$$\frac{1}{t_e(\gamma)} = \frac{1}{E} \left[|a(\gamma)| + \frac{D(\gamma)}{2E} \right], \quad (34)$$

where $a(\gamma)$ and $D(\gamma)$ are the Maxwellian FP coefficients for the equilibrium electron temperature. The physical sense of t_e is that it is the time it takes to change the particle energy considerably (say, by a factor of 2). To obtain the thermalization time scale for a distribution as a whole, one should average $1/t_e(\gamma)$ over the distribution and take the inverse of this value. Applying this to the two thermalization processes considered (Figs. 6 & 7), the power-law has substantially more particles at the higher energy end than the Gaussian, and it therefore has a longer thermalization time, in accordance with Figure 8.

Figure 8 also shows that the equilibrium distribution function does not exactly coincide with the Maxwellian since ε does not go to zero when $t \rightarrow \infty$, but rather stays constant at $\sim 10^{-2}$. This occurs because the differencing scheme (see Eq. 2), modifies the true FP coefficients in order to preserve the energy and number of particles (see Appendix). One can introduce more elaborate energy-dependent corrections to the FP coefficients, and it will likely reduce the deviation ε by an order of magnitude or more. However, since a precision of about 0.01 is satisfactory for our goals, we will leave these improvements to the future.

5. Collision Integrals For Electron-Proton and Electron-Photon Interactions

5.1. Fokker-Planck Coefficients For Electron-Proton Interactions

The fact that electrons and protons are subject to the same Coulomb force as electrons with electrons and electrons with positrons (other than for the cross section) allows us to use the same Fokker-Planck approach as described above to account for these interactions. The FP coefficients for electron-proton (e-p hereafter) scatterings will differ from those of lepton-lepton interactions for the additional reason that the particle masses are no longer the same. In this section, we shall derive the e-p energy exchange $a_p(\gamma, E_p)$ and diffusion $D_p(\gamma, E_p)$ coefficients along the lines established above (E_p is the proton kinetic energy in units of $m_p c^2$). Unlike earlier work in which the FP coefficients were derived for a thermal proton distribution (DL89), we here solve the problem for an arbitrary proton profile.

We follow the same strategy as above and neglect terms of order lower than $\ln \Lambda$ in the final expression. Assuming infinitely massive scatterers (the protons), the e-p differential cross section in the center of momentum frame is

$$\frac{d\sigma^*}{d \cos \Psi^*} = \frac{\pi r_e^2}{2} \frac{1}{\beta_r^4 \gamma_r^2 \sin^4(\Psi^*/2)} \quad (35)$$

(see Jauch & Rohrlich 1980; we neglect the factor $(\beta_r \sin \Psi^*)^2$ compared to unity in the numerator, since we again only include $\Psi^* \ll 1$). The validity of this treatment is limited to $\gamma_r \ll m_p/m_e$, where m_p is the proton mass. The mono-energetic e-p energy exchange coefficient is found to be

$$a_p(\gamma, \gamma_p) = \frac{2\pi r_e^2 c n_p \ln \Lambda m_e}{\beta \gamma^2 \beta_p \gamma_p^2} \int_{\gamma^-}^{\gamma^+} \frac{d\gamma_r \gamma_r^2 S_p^{-1}}{(\gamma_r^2 - 1)^{3/2}} \left[(\gamma_r - 1)(m_p \gamma_p - m_e \gamma) + (m_p + m_e)(\gamma_p - \gamma) \right], \quad (36)$$

where γ_p and γ are the proton and electron Lorentz factors, respectively, $\gamma^\pm \equiv \gamma\gamma_p(1 \pm \beta\beta_p)$, and $S_p \equiv m_p^2 + m_e^2 + 2m_p m_e \gamma_r$. We note that due to the difference in electron and proton masses, $a_p(\gamma, \gamma_p) \neq 0$ even when $\gamma = \gamma_p$. The energy exchange coefficient $a_p(\gamma, \gamma_p)$ is shown in Figure 9 as a function of electron energy, for three different values of the proton energy. Note that there is still a discontinuity at $\gamma = \gamma_p$, however.

The corresponding e-p diffusion coefficient is given by

$$D_p(\gamma, \gamma_p) = \frac{2\pi r_e^2 c n_p \ln \Lambda m_p m_e}{\beta \gamma^2 \beta_p \gamma_p^2} \int_{\gamma^-}^{\gamma^+} \frac{d\gamma_r \gamma_r^2 S_p^{-1}}{(\gamma_r^2 - 1)^{1/2}} \times \left[\frac{(m_p \gamma_p + m_e \gamma)^2}{S_p} - 1 - \frac{[(\gamma_r - 1)(m_p \gamma_p - m_e \gamma) + (m_p + m_e)(\gamma_p - \gamma)]^2}{S_p(\gamma_r^2 - 1)} \right]. \quad (37)$$

To get the e-p FP coefficients for an arbitrary proton distribution $f_p(\gamma_p)$, one integrates Equations (36) and (37) over f_p :

$$a_p(\gamma) = \int_1^{\infty} d\gamma_p a_p(\gamma, \gamma_p) f_p(\gamma_p). \quad (38)$$

We plot the e-p diffusion coefficient for Maxwellian protons with a temperature $kT_p = 10$ MeV and 100 MeV in Figure 10. For comparison, we also show the electron-electron diffusion coefficient for a Maxwellian distribution with $kT_e = 1 m_e c^2$. A graph of the the e-p energy exchange coefficient can be found in DL89. Note that the e-p FP coefficients differ from those of the electron-electron interaction roughly by a factor $(m_e/m_p)T_p/T_e$.

5.2. Electron-Photon Interactions

In this section, we present the electron-photon collision integral corresponding to Compton scattering. This part of the kinetic equation has already been dealt with extensively in the literature (see references below in this section), especially for isotropic photon and particle distributions. With the assumption of isotropy in both the electron and photon spectra, the electron-photon part of the collision integral is

$$\left(\frac{\partial f(\gamma, t)}{\partial t} \right)_{e\gamma} = -f(\gamma) \int d\omega N(\omega) R(\omega, \gamma) + \int \int d\omega' d\gamma' R(\omega', \gamma') P(\gamma; \gamma', \omega') N(\omega') f(\gamma'), \quad (39)$$

where $R(\omega, \gamma)$ is the scattering rate between photons of energy ω and electrons of energy γ ; $P(\gamma; \gamma', \omega')$ is the probability of scattering an electron with initial energy γ' to a final energy γ in a collision with a photon of energy ω' , and $N(\omega) d\omega$ is the number of photons per unit volume with energy between ω and $\omega + d\omega$. For the angle-averaged scattering rate $R(\omega, \gamma)$, we use the expression given in Equation (2.3) in Coppi & Blandford (1990).

The probability $P(\gamma; \gamma', \omega')$ was first derived by Jones (1968) and later corrected by Coppi & Blandford (1990). We carried out the last integral in the expression given by Coppi & Blandford (1990) to get $P(\gamma; \gamma', \omega')$ integrated over all angles. We do not give the rather lengthy expression

since more complete work exists in the literature (e.g., Nagirner and Poutanen 1994 and references therein). We checked the validity of our expression by comparing it with the numerical integrations of Coppi & Blandford (1990) and by integrating $P(\gamma; \gamma', \omega')$ over all the accessible values of γ , which should give unity.

A problem that may arise when Equation (39) is integrated numerically is that the electron energy bin size is finite, which can lead to a situation where scatterings in the low energy regime cannot correctly transfer the particles in energy space. Consider a photon with energy ω (in units of $m_e c^2$) scattering in the Thomson limit, so that $\omega \gamma^2 \ll 1$. The photon emerges with energy $\omega' \sim \gamma^2 \omega$ after one scattering off an electron with a Lorentz factor γ . If the change $\Delta\omega = \omega' - \omega$ in the photon energy is smaller than the electron energy bin size, such a scattering will ‘fall through’ the energy space mesh. When the density of low energy photons is large, the error introduced by this effect can be large.

Because of limited computer resources, it is often impractical to simply reduce the energy bin size. Instead, the photon energy range used in Equation (39) can be divided into 2 sections. Let us define a break energy $\omega_b(\gamma)$ in the photon spectrum by the expression $\omega_b(\gamma) = \min\{\frac{1}{2}(\gamma - 1), 3/(4\gamma)\}$. For low energy photons, that is for $\omega < \omega_b$, we introduce the alternative cooling rate

$$\dot{\gamma}_C(\gamma) \equiv \int_0^{\omega_b(\gamma)} d\omega N(\omega) R(\omega, \gamma) (\langle \omega_s(\gamma) \rangle - \omega), \quad (40)$$

where $\langle \omega_s(\gamma) \rangle$ is the mean scattered energy of the photon ω interacting with an electron with Lorentz factor γ . This cooling rate is in fact the electron-photon energy exchange rate and is analogous to the quantities $a(\gamma, \gamma_1)$ and $a_p(\gamma, \gamma_p)$.

One must also take into account the electron diffusion associated with Compton scatterings, that is the full diffusion coefficient must include a contribution from electron-photon scatterings as well. We define the electron-photon diffusion coefficient as

$$D_C(\gamma) \equiv \int_0^{\omega_b(\gamma)} d\omega N(\omega) R(\omega, \gamma) (\langle \omega_s^2(\gamma) \rangle - \langle \omega_s(\gamma) \rangle^2), \quad (41)$$

where $\langle \omega_s^2(\gamma) \rangle$ is the second moment of the distribution of scattered photons in the scattering of the photon ω and electron γ .

We use the full kinetic equation when the photon energy is $\omega > \omega_b(\gamma)$. In this case, there is no problem with the finite energy bin size because the change in photon energy when these higher frequency photons scatter is large and $\Delta\gamma \sim (\gamma - 1)$. Equation (39) is then written in the form

$$\begin{aligned} \left(\frac{\partial f(\gamma, t)}{\partial t} \right)_{e\gamma} = & - \frac{\partial}{\partial \gamma} [\dot{\gamma}_C f(\gamma, t)] + \frac{1}{2} \frac{\partial^2}{\partial \gamma^2} [D_C(\gamma) f(\gamma, t)] - f(\gamma) \int_{\omega_b(\gamma)}^{\omega_{max}} d\omega N(\omega) R(\omega, \gamma) \\ & + \int_{\omega_b(\gamma)}^{\omega_{max}} d\omega' \int d\gamma' R(\omega', \gamma') P(\gamma; \gamma', \omega') N(\omega') f(\gamma'), \end{aligned} \quad (42)$$

where ω_{max} is the maximum photon energy in the spectrum. To compute both $\gamma_C(\gamma)$ and $D_C(\gamma)$ numerically we use a much finer resolution in photon energy space than that for $\omega > \omega_b(\gamma)$.

We have tested the validity of this approach by first varying the ‘break frequency’ $\omega_b(\gamma)$ and found that the variations in the results are always much smaller than the chosen relative variation in $\omega_b(\gamma)$. We also varied the number of bins N for a fixed electron energy range and found that this too makes a negligible difference on the results. These tests would unambiguously point to inconsistencies if they were there.

Finally, for pair annihilation we use the rate $R(\gamma_-, \gamma_+)$ given by Svensson (1982), where γ_- and γ_+ are electron and positron gamma-factors, respectively. For pair creation we adopt the expressions in Coppi & Blandford (1990).

6. Tests

6.1. The Full Equation

Our goal in this section is to demonstrate the use of the self-consistent FP approach in the treatment of photon-particle interactions in astrophysical plasmas. Situations where one can assume that a part of the distribution is Maxwellian have been studied in some detail for the case of non-thermal models (e.g, Zdziarski et al. 1990; Svensson 1994, and references cited therein). Ghisellini, Guilbert & Svensson (1988) studied the thermalization of the low energy end of the non-thermal distribution by synchrotron reabsorption; they neglected e-e Coulomb and inverse Compton interactions. DL89 developed a perturbative approach to the FP equation for e-e Coulomb interactions, but have not applied the method to problems that require finding the photon distribution self-consistently.

We first present the complete equation, including all the processes discussed above, i.e., Coulomb and Compton interactions, as well as pair creation and annihilation. We shall not here attempt to make a detailed study of the various applications, which would require a careful examination of source geometries and a thorough search in parameter space. This subject is vast and will be covered in future publications.

All the distributions are assumed to be spatially uniform inside of a spherical volume with radius R . Since the number of positrons is always different (i.e., smaller) than the number of electrons, the positron distribution is never identical to that of the electrons. This is true even though the electron-electron and electron-positron cross sections are the same within the scope of the approximation we use here (see §4.1). The processes that shape these particle profiles differently include pair annihilation and, when included, bremsstrahlung emission and pair escape. In the following, we neglect the contribution of bremsstrahlung to the overall photon production, assuming instead that the soft photons are injected by an external source. Index 1 will be used to denote electrons, whereas 2 pertains to positrons.

The full equation for the electrons reads

$$\begin{aligned} \left(\frac{\partial f_1(\gamma, t)}{\partial t}\right) &= -\frac{\partial}{\partial E} \left[A(\gamma) f_1(\gamma, t) \right] + \frac{1}{2} \frac{\partial^2}{\partial E^2} \left[D(\gamma) f_1(\gamma, t) \right] + \\ &+ \left(\frac{\partial f_1(\gamma, t)}{\partial t}\right)_{e\gamma} - R_1(\gamma) f_1(\gamma, t) + S(\gamma), \end{aligned} \quad (43)$$

where $A(\gamma)$ is the total energy exchange rate for an electron with Lorentz factor γ ; that is, $A(\gamma)$ is the sum of energy exchange rates from processes which can be treated using a Fokker-Planck approach. This excludes inverse Compton interactions which are instead incorporated into the term $(\partial f_1(\gamma, t)/\partial t)_{e\gamma}$, as given in §4.2. Similarly, $D(\gamma)$ is the electron diffusion coefficient, a sum of the electron-electron, positron-electron and proton-electron diffusion coefficients.

The function $R_1(\gamma)$ is the electron annihilation rate,

$$R_1(\gamma) = \int_1^{\infty} d\gamma_2 f_2(\gamma_2) R(\gamma, \gamma_2), \quad (44)$$

where $R(\gamma, \gamma_2)$ is the angle-averaged annihilation rate for an electron with energy γ and positron with energy γ_2 as given by Svensson (1982). $S(\gamma)$ is a ‘source’ term that represents pair production by photon-photon collisions. The pair creation rate is an integral over the photon distribution $N(\omega, t)$ as given by Coppi & Blandford (1990).

The full equation for the positrons has an identical form, except that the subscripts 1 and 2 are interchanged. The often used quantitative measure of the heating power going into electrons is the dimensionless ‘hard’ compactness parameter

$$l_h = \frac{4\pi R^2 \sigma_T}{3c} \int d\gamma A^+(\gamma, t) [f_1(\gamma, t) + f_2(\gamma, t)], \quad (45)$$

where $A^+(\gamma, t)$ is the energy and time dependent heating rate for an electron/positron with energy γ . For the proton heating rate given by Equation (38), the time dependence results from the change of the proton temperature in time. Letting l_h represent the energy transfer rate to the protons (due to dissipational processes), the proton temperature is then found by balancing this heating and the Coulomb cooling by cold electrons at every instant in time.

The equation for the photons reads

$$\frac{\partial N(\omega)}{\partial t} = \dot{N}(\omega) - \left(\frac{\partial N(\omega)}{\partial t}\right)_{e\gamma} + P(\omega) - N(\omega)/t_{esc}(\omega), \quad (46)$$

where $\dot{N}(\omega)$ is the rate of external photon injection (photons are here assumed to be injected uniformly in space throughout the plasma containing region), $P(\omega)$ is the number of photons with energy ω created per unit time per unit volume per unit energy by pair annihilation, and $t_{esc}(\omega)$ is the photon escape time as given by Lightman & Zdziarski 1987:

$$t_{esc}(\omega) = \frac{R}{c} [1 + (1/3) \phi(\omega) \tau_{KN}(\omega)], \quad (47)$$

in terms of the size R of the region. The energy dependent optical thickness $\tau_{KN}(\omega)$ is here defined by

$$\tau(\omega) = \tau_T \sigma_{KN}(\omega) / \sigma_T,$$

where $\tau_{KN}(\omega)$ is the Klein-Nishina cross-section (see, e.g., Jauch and Rohrlich 1980, Eq.[11.24]). The function $\phi(\omega)$ takes into account the fact that forward scattering for high energy photons becomes important (see Lightman and Zdziarski 1987; Equation [21b]). We should mention that

this treatment of the photon radiative transport is only approximate, especially for a low optical depth. However, the solution found this way will undoubtedly bear the same qualitative imprints of the ‘exact’ electron distribution as the still to be found solution which includes *both* radiative transport for the photons and the FP treatment of the electrons.

The term $[\partial N(\omega)/\partial t]_{e\gamma}$ represents the full Compton interaction with electrons and positrons and is given by the collision integral

$$\begin{aligned}
 -\left(\frac{\partial N(\omega)}{\partial t}\right)_{e\gamma} &= -N(\omega) \int_0^\infty d\omega' \int_1^\infty d\gamma R(\omega, \gamma) [f_1(\gamma) + f_2(\gamma)] \\
 &+ \int_0^\infty d\omega' \int_1^\infty d\gamma' P(\gamma, \gamma', \omega') R(\omega', \gamma') N(\omega') [f_1(\gamma') + f_2(\gamma')], \quad (48)
 \end{aligned}$$

where $R(\omega, \gamma)$ and $P(\gamma, \gamma', \omega')$ are defined in §4.2, and $\gamma + \omega = \gamma' + \omega'$.

In the tests reported here, we take the photon injection rate $\dot{N}(\omega)$ to be that of a blackbody spectrum with dimensionless temperature $\Theta_b \equiv kT_b/m_e c^2$ in the range $\Theta_b = 10^{-5} - 10^{-4}$. This injection rate is characterized by the dimensionless ‘soft’ photon compactness parameter (e.g., Lightman & Zdziarski 1987)

$$l_s = \frac{4\pi R^2 \sigma_T}{3c} \int d\omega \omega \dot{N}(\omega). \quad (49)$$

We also need to specify the electron heating mechanism. It is well known (Guilbert, Fabian & Stepney 1982), that the electron-proton Coulomb interactions are very inefficient, and if cooling is effective, it is impossible to account for the observed high electron temperature $\Theta_e \gtrsim 0.2$ observed in Seyfert Galaxies, as implied by their high exponential cutoff energy (e.g., Svensson 1996 and references therein). One then needs to introduce some *ad hoc* heating mechanism for the electrons. Many workers do not specify the mechanism by which the energy is transferred to the electrons and instead specify the heating rate per electron (independent of the electron energy) per unit volume. This is indeed the only information needed if one assumes that the particles are thermal.

However, for our purposes we need to know the diffusion coefficient for this heating interaction. Since it is beyond the scope of this paper to explore the full range of interactions that heat the electrons in real astrophysical plasmas, we model the electron heating by the e-p Coulomb interactions with a fixed proton temperature, $kT_0 = 20$ MeV, but in addition, we multiply this interaction (both the energy exchange and diffusion) by a factor (equal to T_p/T_0 , see § 6.4.c) which is needed to account for the electron heating rate given by the specified l_h . While this is obviously a non-physical interaction, it will allow us to make some progress in understanding what one can expect to happen with the electron distribution. It also will allow us to have a ‘reference scale’; whether the electron distribution is actually broader or narrower than the one found in this test model depends on whether the actual electron heating mechanism produces comparatively more or less diffusion.

6.3. Results

In this section we apply our technique to a test situation where the electrons and positrons are heated by some external source as described in section 6.1, and cooled by inverse Compton

scatterings with soft intense external radiation. The description of the numerical procedure used to solve for the exact electron distribution can be found in Appendix A.3. Ghisellini, Haardt and Fabian (1993) (GHF hereafter) have shown that the exact shape of the electron distribution produces very little effect on the photon spectra as long as the *multiple* Compton scatterings are the main emission mechanism. In particular, they considered three different particle distributions that had the same normalization and the same value of $\langle \gamma^2 - 1 \rangle$: a Maxwellian, a power-law, and a constant (i.e., $f(\gamma) = \text{const}$). The resulting spectra were hardly distinguishable.

We conduct similar tests here. For the test electron distribution, we choose: 1) the exact electron distribution found by using the techniques developed in this paper; 2) a Maxwellian; 3) a distribution broader than a Maxwellian (see Figs. 11a and 12a). In the last case, the functional shape of the distribution function is given by $f(E) = \text{const} \sqrt{f_{\text{mxw}}(E, \Theta_e)}$, where $f_{\text{mxw}}(E, \Theta_e)$ is a Maxwellian distribution with temperature Θ_e . Just like in the familiar Maxwellian case, there are again two parameters, Θ_e and the normalization, which are found self-consistently. One very important difference of our tests from those of GHF is that we find the equilibrium pair number density by solving the exact pair balance, so that the relative positron number density, $z \equiv n_+/n_p$, is different for the three tests. This results in a different optical depth for the different distributions, even though the proton optical depth τ_p is the same for all three.

We first discuss the photon spectra. Figures 11b and 12b show the photon spectra for $l_h = l_s = 420$, $\tau_p = 0.05$ and $l_h = 8.4$, $l_s = 2.1$, $\tau_p = 0.02$ respectively. The input and output parameters of these tests are given in Table 1. For the case of the higher optical depth (Fig. 11b), it is readily seen that the spectrum does not vary much from one case to another, at least in the X-ray energy range (2-18 keV). This is similar to the findings of GHF, and is explained by the fact that the spectrum is formed by many repeated scatterings, which simply form a power-law after two to three interactions.

However, for the second test our results disagree with conclusions of GHF. We find qualitative differences between the Comptonized spectra produced by the three test electron distributions (Fig. 12b). The difference with GHF is caused by the fact that the calculated here exact electron distribution is narrower than a thermal one (Fig. 12a), and also that we test the parameter space with a lower optical depth. GHF considered only a subset of the parameter space available for the distribution function; they only considered cases where the electron distribution is broader, more diffuse than the thermal distribution. At the present, it is completely unclear if this is indeed what happens. The answer to the question regarding the electron distribution function can only be given if one specifies the interactions affecting the electrons.

6.4. The Strongly Non-Maxwellian Electron Distribution

a. The electron distribution profile

Using the tests described below as examples, we will discuss the parameter space where λ is much larger than unity, i.e., where strongly non-thermal distributions are expected. Figures 11a and 12a show the three test electron distributions for the tests described in 6.3 ($\lambda \simeq 80$ and 10 for the two figures, respectively). The exact electron distributions are shown as solid curves, and are much sharper than the thermal electron distribution (dashed line). For the parameter space considered here, the electrons with energy $E \ll \langle E \rangle$, where $\langle E \rangle$ is the electron average energy,

interact mostly with protons which strive to push these electrons to higher energy. The electrons with energy $E \gg \langle E \rangle$, similarly interact mostly with photons. Therefore, the electron distribution appears to be squeezed by the photon cooling on the high energy end and the proton heating on the low energy end (see Fig. 13).

As surprising as this might sound, the exact distributions in Figures 11a) and 12a) are actually as simple to find as the familiar Maxwellian distribution (corresponding to the given compactnesses and τ_p). The FP part of the full electron Equation (43) is by far the dominant one. That means that the actual shape of the particle distributions is controlled by the FP part, while the normalizations are governed by the much slower annihilation and creation processes. Thus we can find the shape of the distributions solving just the stationary FP equation. Furthermore, for $\lambda \gg 1$, both electron heating and cooling greatly exceed the e-e Coulomb interactions (for an example see Fig. 13). Essentially, the FP equation becomes linear in the electron distribution function, which greatly simplifies the solution of this equation. The stationary (i.e., with zero time derivative) FP Equation (8) has then an exact solution:

$$f(\gamma) = \frac{\text{const}}{D(\gamma)} \exp \left[2 \int_1^\gamma d\gamma' [A(\gamma')/D(\gamma')] \right]. \quad (50)$$

We have dropped subscripts 1 and 2 on the distribution function since in this approximation the positron distribution has the same shape as that of the electrons, and only the normalization is different.[†]

Figure 14 shows the exact distribution (same as in Fig. 12a) and various fits to it. The heavy dashed curve shows the function given by Equation (50) when $A(\gamma)$ and $D(\gamma)$ include all the interactions. The larger dots show the same Equation (50) but with the e-e interactions excluded, i.e., the linear case. As one can see, both fits are very good. And the faint dotted curve gives an analytic fit to Equation (50).

We now explain this fit. Figure 13 shows all the FP coefficients for the test previously shown in Fig. 12. Notice that the proton diffusion coefficient is almost a constant, so we can approximate $D(\gamma) \simeq D(\gamma_0) \equiv D_0$ (where γ_0 is the point where electron cooling is equal to electron heating). We also approximate the electron-proton energy exchange coefficient as a constant, $A^+(\gamma) \simeq A_0 \equiv A^+(\gamma_0)$, which should be sufficiently accurate around the peak energy E_0 (see the Figure). Using the fact that $A^-(\gamma) \propto \beta^2 \gamma^2$, we can write $A(\gamma) \simeq A_0 [1 - (\beta\gamma/\beta_0\gamma_0)^2]$. Using this expression in (50), we get

$$f(\gamma) \simeq \text{const} \exp \left[\frac{2A_0}{\beta_0^2 \gamma_0^2 D_0} (\gamma_0^2 \gamma - \gamma^3/3) \right]. \quad (51)$$

Notice that this expression is also quite accurate around the peak of the exact distribution function, but deviates on the low energy end. This deviation will be negligible for the distribution as a whole if the electron heating is more or less energy independent.

[†] This similarity in the electron and positron distributions exists in the exact simulations as well, and we therefore do not show the positron curves in Figures 11a & 12a.

One can easily show that the dispersion of the electron distribution, defined as $\langle \Delta\gamma \rangle \equiv [(\langle \gamma - \gamma_0 \rangle)^2]^{1/2}$, where the averaging is taken over the electron distribution, is

$$\langle \Delta\gamma \rangle \simeq \left[\frac{\gamma_0 \beta_0^2 D_0}{A_0} \right]^{1/2} \quad (52)$$

Therefore, for the same heating rate (which will lead to the same γ_0), it is the diffusion coefficient that determines the dispersion of the distribution. Physical conditions under which the ‘wide’ electron distribution might form can now be understood in terms of a very large diffusion coefficient which might result from some particular form of the electron interaction.

6.4.b. Normalization of the electron distribution

The electron-positron annihilation rate depends rather weakly on the energy of the colliding particles as long as their energy is smaller than a few MeV (e.g., Coppi and Blandford 1990, Equation 3.7). Therefore, the exact particle profile does not change the pair annihilation rate substantially. Nevertheless, its importance shows up in the shape of the photon spectra around the pair producing energy (see Figs. 11b and 12b). We can indirectly find the equilibrium pair number density by considering the Compton y -parameter (see, e.g., Rybicki and Lightman 1979). It is defined as

$$y \equiv \langle G \rangle \langle t_{\text{esc}} \rangle / t_T, \quad (53)$$

where $\langle G \rangle$ is the average fractional gain in the photon energy in one scattering, $\langle t_{\text{esc}} \rangle$ is the average escape time and t_T is the Thomson time. By definition, the electron cooling rate is $(dE/dt)^- = c\sigma_T \langle G \rangle U_{\text{ph}}$, where U_{ph} is the photon energy density in the source. In equilibrium, the total electron heating, L_h , equals the total cooling, so that

$$L_h = V_0 n_p (1 + 2z) (dE/dt)^- = c\sigma_T n_p (1 + 2z) \langle G \rangle V_0 U_{\text{ph}}. \quad (54)$$

where V_0 is the source total volume and $z \equiv n_+/n_p$, ratio of positron number density to that of protons. Using Equation (53) and the fact that $L = U_{\text{ph}} V_0 / \langle t_{\text{esc}} \rangle$, where $L = L_h + L_s$ is the total luminosity of the source, we get

$$y = \frac{L_h}{L_h + L_s}. \quad (55)$$

This derivation did not make any use of the particular shape of the electron distribution, and therefore is valid for an arbitrary one, as long as the inverse Compton scattering is the main mechanism for the transfer of energy from the particles to the escaping photons. We note that the numerical value predicted by Equation (55) should be corrected by taking into account relativistic Klein-Nishina decline in the Compton cross section. The principal effect then is to reduce L_h in the denominator, since these are the photons that have largest energies. This correction is rather trivial to do, and we leave it to the reader.

Now, since we know the electron distribution shape (Eq. 50), we can find $\langle G \rangle$ by simple convolution of this shape with the particle-photon energy exchange rate. Equations (55) and (53) then determine the Thomson optical depth and so the desired normalization of the electron

distribution. This is particularly simple for the Thomson scattering limit, e.g., for a spherical geometry,

$$y \simeq \tau_T(1 + \tau_T/3)(4/3)\langle\beta^2\gamma^2\rangle. \quad (56)$$

For the tests shown in Figure 11, the y -parameter must equal 1/2. Numerically finding $\langle\beta^2\gamma^2\rangle$ in Equation (56), we get $y = 0.5 \pm 0.01$ for all three tests.

We have shown that, once the electron energy exchange and diffusion coefficients are known, it is a simple matter to find the electron distribution. Although we have considered only systems where the electron cooling is dominated by the Comptonization of the soft external photons, one can extend the methods described here to more complicated situations. We intend to cover this in future publications.

6.4.c. Proton temperature

The last column in Table 1 shows the equilibrium proton ‘temperature’. We define the proton temperature such that the e-p heating is equal to $(T_p/T_0) a_p(\gamma, T_0)$, and $kT_0 = 20$ MeV. For both tests, we see that T_p varies from distribution to distribution, and the pattern is such that the more diffuse the distribution is, the colder the protons become.

The explanation for this is rather straightforward. The e-p energy exchange rate (see Fig. 9 in this paper and Fig. 10 in DL89) is a decreasing function of the electron energy. It is mostly the low energy electrons that are heated by the e-p interactions. Since more diffuse distributions have more electrons at low energy, they absorb more energy per electron from the hot protons. Additionally, we also saw in the tests we conducted that the more diffuse distributions are associated with the larger optical depths. That is, there are more leptons per proton, which again lowers the proton temperature.

Yet another consequence of the change in the electron distribution function is an associated change in the proton cooling time scale. Let us define this time scale by the equality $E_p/t_p \equiv A_p$, where A_p is the proton cooling rate, and E_p is the proton average energy. Assume that the proton heating rate (e.g., from the dissipation of gravitational energy) is a constant. Then A_p is independent of the electron distribution, since proton cooling and heating are equal to each other in equilibrium. Also, $E_p \propto T_p$, the proton temperature, and thus the proton cooling time scale is directly proportional to this temperature.

Even though we here assume a non-physical form for the proton heating, it is quite likely that a similar result will hold for real interactions that transfer energy from the hot protons to the electrons in astrophysical plasmas. Indeed, the e-p energy exchange rate must be a decreasing function of the electron energy, since after all it must become negative after the electron energy surpasses that of the protons. The second part of the argument, based on the change in lepton number, holds true irrespective of the exact nature of the e-p interaction. Finally, the proton cooling time scale will remain unchanged only when the proton-electron energy transfer rate is independent of the proton energy, which is rather unlikely.

8. Conclusions

We have presented the general FP method for finding the electron distribution in non-Maxwellian hot, isotropic plasmas. The technique can be applied to both time dependent and

stationary problems. Approximate expressions (Equations 50 and 51) for the exact electron distribution function are developed. These approximate expressions enable one to find the exact electron distribution in about the same number of steps as is required to find the temperature and equilibrium number density for a Maxwellian electron distribution.

A simple parameter (§ 2) specifies the section of the parameter space where the treatment presented here is important. In general, this occurs for optically thin, mildly relativistic and relativistic plasmas that are not too strongly magnetized. Two representative tests show that the parameter space is further divided into two regions (the exact boundary between these two regions depends on the particle distribution and the as-yet-unknown physics of electron heating; we intend to investigate this boundary in future work). In the first region the exact shape of the electron distribution does not influence the produced photon spectra, which are close to power-laws. While this finding agrees with the work of GHF, we find that the difference in the electron profile can lead to different equilibrium pair number densities. This fact will be important in the radiation pressure dominated plasmas, since the radiative pull on the protons is proportional to the number of leptons per proton ($\equiv 1 + 2z$). Of equal importance is the change in the proton temperature. A smaller proton temperature increases the importance of the radiation pressure, and for the tests we have presented here, the combined effect is such that the ratio of radiation pressure to the proton pressure changes by more than a factor of 10 from the exact to the ‘wide’ distribution. With such a large difference in this ratio, there can be situations where the plasma can be either gas or radiation dominated depending on what distribution electrons have. Therefore, we conclude that it is probable that the equilibrium (including hydrostatic) plasma state will still be sufficiently different for different particle distributions to produce noticeable differences in the photon spectrum; this question needs to be investigated further.

In the other, generally optically thinner, region, the photon spectra bear strong imprints of the exact shape of the particle distribution, and are not simple power-laws. The local X-ray index and break energies depend on the exact particle profile. Use of the exact electron distribution can then limit the parameter space for a particular astrophysical model differently than the use of the thermal distribution does.

A shortcoming of this paper is the use of the diffusive escape time approximation (Equations 46, 47) instead of the exact radiation transport approach (e.g., Poutanen and Svensson 1996). One can, however, include radiation transport in the same way as is done for Maxwellian electrons. We anticipate that the ‘non-power-law’ features in the photon spectra may be even stronger with the inclusion of radiation transport. Our treatment of radiation employed the angle averaged corrected Jones expression for the Compton scattering. If one is fixing the viewing angle instead, the amount of dispersion in the photon upscattered energies become smaller (because one angle average is removed), and the spectra will track the electron distribution better.

Another interesting question, which should be addressed in future work, is whether there are generic limits on the ratio of the electron heating diffusion coefficient to the energy exchange one, independent of the exact interaction which heats the electrons. If this is so, then we should be able to determine just how much the exact electron distribution can be broader or narrower than a Maxwellian.

C. Dermer provided us with his own differencing scheme which helped us to develop the scheme presented in this paper. We are grateful to M. Boettcher for a stimulating discussion of the importance of the different terms in the electron-electron diffusion coefficient. We are also grateful to the anonymous referee for his careful reading of the manuscript and making many suggestions that have greatly improved the paper. This work was supported in part by NASA grants NAGW-2709 and NAG 5-3075.

Figure Captions

Figure 1. Coulomb energy exchange coefficient $a(\gamma, \gamma_1)$ for a test particle scattering off a mono-energetic electron distribution (i.e., $f(\gamma) = \delta[\gamma - \gamma_1]$) for three different values of γ_1 . The curves are labeled by their corresponding values of γ_1 . The Coulomb logarithm here and throughout the paper is set to 20. The time t_C is defined as $t_C \equiv (n_e c \sigma_T \ln \Lambda)^{-1}$, and n_e is the total lepton number density.

Figure 2. Coulomb diffusion coefficient $D(\gamma, \gamma_1)$ for a test particle scattering off a mono-energetic electron distribution (i.e., $f(\gamma) = \delta[\gamma - \gamma_1]$) for three different values of γ_1 . The curves are labeled by their corresponding values of γ_1 .

Figure 3. The electron energy exchange coefficients $a(\gamma)$ for three different electron distributions (plotted in Fig. 5 below). The solid curve corresponds to a Maxwellian distribution with temperature $\Theta_e \equiv kT_e/m_e c^2 = 1$. The distributions have the same average energy and are normalized to unity. The dotted and dashed curves correspond to a power-law ($f(\gamma) = \beta\gamma^{-p}$; $p = 2.48$) and a Gaussian, respectively.

Figure 4. The electron diffusion coefficient $D(\gamma)$ for the same distributions as in Figure 3.

Figure 5. The three electron distributions used to compute the FP coefficients plotted in Figures 3 & 4. All three functions are normalized to unity and have the same average energy. Solid, dotted and dashed lines correspond to Maxwellian, power-law and Gaussian distributions, respectively. The temperature of the Maxwellian is $\Theta_e = 1$.

Figure 6. Time evolution of an initial power-law ($f(\gamma) = \gamma^{-p}$; $p = 3.72$) distribution of electrons coming into equilibrium (i.e., approaching a Maxwellian distribution) via Coulomb interactions with itself. The temperature of the equilibrium Maxwellian is 0.3. The box on the left shows the time corresponding to each curve (t_C is defined in the caption of Fig. 1). The solid curve with $t = \infty$ corresponds to the perfect Maxwellian. Note that our choice of times to plot $f(\gamma, t)$ was dictated by convenience of viewing and not by equal spacing in time. In fact, thermalization is always *slower at later* times.

Figure 7. The same as Figure 6 except that the initial distribution is a Gaussian with the mean energy corresponding to a Maxwellian temperature of $0.3 m_e c^2$.

Figure 8. Time evolution of ε (defined in Eq. 32), the deviation from a perfect Maxwellian. Solid and dotted lines correspond to thermalization of the power-law (Fig. 6) and Gaussian (Fig. 7). Note the Gaussian relaxes to the thermal distribution much faster than the power-law. For comparison, the electron-electron thermalization time scale given by Equation (33) is $0.06 t_T$ for the given equilibrium temperature of 0.3.

Figure 9. The mono-energetic electron-proton energy exchange coefficient $a_p(\gamma, \gamma_p)$ as a function of the electron energy. The curves are labeled by their corresponding values of the proton kinetic energy.

Figure 10. The electron-proton diffusion coefficient for the case of Maxwellian protons. The Maxwellian electron-electron diffusion coefficient for $\Theta_e = 1$ is shown with a dashed line for comparison (same as the solid curve in Fig. 4).

Figure 11. a) The equilibrium electron distributions for the tests described in section 6.3. The parameters are: $l_h = l_s = 420$, $\tau_p = 0.05$ (also see Table 1). The exact distribution is the solution of the full kinetic equation, which includes electron heating, cooling and pair creation and annihilation. The Maxwellian curve is the solution of the same problem but assuming that the distribution is thermal. The ‘wide’ electron distribution is again a solution of the same problem, but assuming a wider than thermal profile for the distribution. The three distributions have a different ‘temperature’ and number of particles, but produce almost identical spectra (Fig. b). **b)** The photon spectra corresponding to the electron distributions plotted in Fig. 11a.

Figure 12. a) The same as Fig. 11a, but now for $l_h = 8.4$, $l_s = 2.1$, $\tau_p = 0.02$. **b)** The corresponding photon spectra. Notice that the spectra are distinctly different from each other, and are not simple power-laws anymore. See Table 1 for additional information about input and output parameters.

Figure 13. a) The electron energy exchange coefficients plotted for the tests shown in Fig. 12. The solid, dotted and dashed curves show the electron-photon cooling (the dominant FP part, see § 4.2), e-p heating and e-e energy exchange coefficients. **b)** Same as **a)**, but for the electron diffusion coefficients. Note that both energy exchange and diffusion are dominated by electron-photon or electron-proton interactions.

Figure 14. Various fits to the exact electron distribution (shown with the solid curve) for the test presented in Fig. 12. The dashed curve corresponds to the function given by Equation (50) with all the FP coefficients included, and the big dotted curve corresponds to the solution with the electron-electron FP coefficients excluded. The ‘faint’ dashed curve shows the fit given by the simple expression in Equation (51). See text for details.

Table 1. The output and input parameters for the tests presented in section 6.3 and plotted in Figures 11 & 12.

Model ^a	l_h	l_s	τ_p	Θ_b	τ_T^b	$\langle E \rangle^c$	kT_p^d (MeV)
exact	420	420	0.05	10^{-4}	0.22	0.58	2400
wide	420	420	0.05	10^{-4}	0.41	0.29	190
thermal	420	420	0.05	10^{-4}	0.27	0.48	1100
exact	8.4	2.1	0.02	3×10^{-5}	0.14	1.46	440
wide	8.4	2.1	0.02	3×10^{-5}	0.20	0.87	53
thermal	8.4	2.1	0.02	3×10^{-5}	0.17	1.27	240

^a The assumed or exactly determined shape of the electron distribution (see § 6.3). The next four columns give the input parameters for the various models: hard and soft compactness (Eq. 50 & 54, respectively); τ_p , the ‘proton optical depth’; the injected blackbody photon temperature, $\Theta_b \equiv kT_b/m_e c^2$.

^b Thomson optical depth of the plasma, $\tau_T \equiv \tau_p(1 + 2z)$, where z is the ratio of positron number density to that of the protons.

^c Average electron energy.

^d Proton ‘temperature’, defined in § 6.4.

Note that differences in the equilibrium optical depth, and the electron and proton ‘temperatures’ occur even when the radiation spectra are almost indistinguishable.

References

- Baring, M. 1987, *M.N.R.A.S.*, 228, 695
- Boettcher, M. 1996, private communication.
- Cameron, R.A. et al. 1995, Proc. of the Compton Symp., ed. N. Gehrels, in press
- Chandrasekhar, 1942, S. Principles of Stellar Dynamics (Chicago: UC Press), p. 89
- Coppi, P.S. & Blandford, R.D., 1990, *M.N.R.A.S.*, 245, 453-469
- Dermer, C. D., 1985, *Ap. J.*, 295, 28
- Dermer, C.D., 1984, *Ap. J.*, 280, 328
- Dermer, C. D. & Liang, E.P., 1989, *Ap. J.*, 339, 512-528 (DL89)
- van Dijk, R. et al. 1995, *A&A*, 296, L33
- Fabian, A.C. 1994, *Ap. J.* Supplement Series, 92, p. 555
- Guilbert, P.W., Fabian, A.C. & Stepney, S. 1982, *MNRAS*, 199, 19p
- Ghisellini, G., Guilbert, P. & Svensson, R. 1988, *Ap. J.*, 334, L5-L8
- Ghisellini, G., Haardt, F. & Fabian, A.C. 1993, *MNRAS*, 263, L9 (GHF)
- Guilbert, P. W., and Stepney, S. 1985, *M.N.R.A.S.*, 212, 523
- Guilbert, P.W., Fabian, A.C. & Stepney, S. 1982, *MNRAS*, 199P, 19
- Haardt, F. & Maraschi, L. 1991, *ApJ*, 380, L51
- Haardt, F. & Maraschi, L. 1993, *ApJ*, 413, 507
- Haardt, F., Maraschi, L. & Ghisellini, G. 1994, *ApJ*, 432, L95
- Haardt, F., Maraschi, L. & Ghisellini, G. 1996, *ApJ*, submitted.
- Jauch, J.M., and Rohrlich, F., 1980, *The Theory of Photons and Electrons* (New York: Springer)
- Jones, F.C., 1968, *Phys. Rev.D*, 167, 1159
- Johnson, W.N., et al. 1993, *A&AS*, 97, 21
- Kompaneets, A.S. 1957, *Sov. Phys. JETP*, 4, 730
- Kusunose, M. 1987, *Ap. J.*, 321, 186
- Landau, L. & Lifshitz, E., *Physical Kinetics*, volume 10 of *Course of Theoretical Physics*, Pergamon Press, 1981.
- Li, Hui, Kusunose, M. & Liang, E.P. 1996, *ApJ Letters*, 460, L29
- Liang, E.P. 1979, *Ap. J.*, 234, 1105
- Lightman, A.P. & Zdziarski, A.A. 1987, *Ap. J.*, 319, 643
- Ling, J.C., Mahoney, W.A., Wheaton, Wm. A. & Jacobson, A.S. 1987, *ApJ*, 321, L117
- Madejski, G. et al. 1995, *Ap. J.*, submitted
- Maisack, M. et al. 1993, *Ap. J.*, 407, L67
- McConnell, M., et al. 1994, *ApJ*, 424, 933
- Melia, F. & Misra, R. 1993, *Ap. J.*, 411, 797
- Misra, R. & Melia, F. 1996, *ApJ*, 467, 405
- Nagirner, D.I., & Poutanen, J. 1994, *Astrophys. Space Phys. Reviews*, Vol. 9, 1-83
- Nayakshin & Melia, “Physical Constraint on Active Regions in Seyfert Galaxies, in preparation”, 1997a

- Nayakshin & Melia, “Magnetic flares and observed $\tau_T = 1$ in Seyfert Galaxies”, submitted to ApJL, 1997b
- Poutanen, J., & Svensson, R. 1996, *Ap. J.*, in press
- Press, W.H., Flannery, B.P., Teukolsky, S.A. & Vetterling, W.T. 1986, Numerical Recipes (New York: Cambridge)
- Rybicki, G. B. & Lightman, A.P., 1979, Radiative Processes in Astrophysics, Wiley-Interscience Publication
- Shapiro, S.L., Lightman, A.P. & Eardley, D.M. 1976, *Ap. J.*, 204, 187
- Stepney, S., 1983, *M.N.R.A.S.*, 202, 467
- Sunyaev, R.A. & Titarchuk, L. 1980, A&A, 86, 121
- Sunyaev, R.A. et al. 1991, *Sov. Astron. Letters*, 17, 409
- Svensson, R. 1982, *Ap. J.*, 258, 335
- Svensson, R. 1990, in Proc. NATO Advanced Research Workshop on Physical Processes in Hot Cosmic Plasmas, ed. W. Brinkmann (Dordrecht: Kluwer), 357
- Svensson, R., 1994, ApJS, 92, 585
- Svensson, R., 1996, A&A, in press.
- Titarchuk, L. 1994, ApJ, 434, 570
- Titarchuk, L. & Mastichiadis, A. 1994, ApJ, 433, L33
- Zdziarski, A.A., Coppi, P.S. & Lamb, D.Q. 1990, *Ap. J.*, 357, 149
- Zdziarski, A.A. et al. 1994, MNRAS, 269, L55
- Zdziarski, A.A., Johnson, W.N., Done, C., Smith, D. & McNaron-Brown, K. 1995, ApJ, 438, L63

Appendix

A.1 The Finite Differencing scheme

Finding a numerical scheme to solve Equation (8) that is stable and preserves the essential physics (i.e., one that conserves the particle number and energy, and that leads to a perfect Maxwellian in equilibrium) can be a non-trivial problem. We shall mention that the need to conserve the number and energy is not simply an aesthetic goal, but comes rather from a need to address practical problems involving pairs, photons and protons (see § 6). When the escape rate of particles becomes small (i.e., when the optical depth is large), we find severe problems with all differencing schemes that do not conserve the energy and number “exactly”. In particular, unphysical pair runaways may ensue. We shall therefore present the energy and particle conserving scheme in detail. The scheme we have settled on is

$$f_k^{n+1} = f_k^n - \Delta t \left(\frac{a_{k+1}^n f_{k+1}^n - a_{k-1}^n f_{k-1}^n}{\Delta x_{k-1} + \Delta x_k} \right) + \frac{s}{2} \left[\alpha D_{k+1}^n f_{k+1}^n - 2D_k^n f_k^n + \rho D_{k-1}^n f_{k-1}^n \right], \quad (\text{A1})$$

where

$$s \equiv \frac{2\Delta t}{\alpha \Delta x_k (\Delta x_{k-1} + \Delta x_k)}. \quad (\text{A2})$$

Here $a(E)$ and $D(E)$ are the energy exchange and diffusion FP coefficients, respectively, which are given as integrals over the distribution function f itself.

The index k refers to the energy (x_k is a point in energy space), and n denotes the time. The parameters α and ρ have been introduced to make sure the scheme preserves the particle normalization and energy. In our calculations, we have chosen a logarithmic energy spacing, and one can show in this case that in order to preserve these aspects, one must choose

$$\alpha = \frac{2}{1+q}, \quad \rho = \frac{2q}{1+q}, \quad (\text{A3})$$

where $q = x_{k+1}/x_k$. To demonstrate that this must be the case, we need only consider a numerical realization of the integrals $\int dE [f^n(E) - f^{n+1}(E)]$ and $\int dE E[f^n(E) - f^{n+1}(E)]$ for the evolving distribution, and require these to give zero.

Because Equation (8) is a flux equation, a sensible constraint to impose at the boundary is a mirror condition at both the low and high energy ends. This means modifying the differencing scheme (Eq. A1) for a few boundary points. We explicitly set the value of the distribution function in the first and last points to zero. That means that the two extreme points in the actual distribution function should be far enough from the maximum of the distribution that neglecting the (small) number of particles in the boundary bins does not introduce a noticeable error. Requiring the total number of electrons to not change with time, one obtains certain conditions on the differencing scheme at the neighborhood of the boundaries. These conditions lead us to choose the differencing scheme for the second point on the energy axis to be

$$f_2^{n+1} = f_2^n - \Delta t \left(\frac{a_3^n f_3^n + a_2^n f_2^n}{\Delta x_1 + \Delta x_2} \right) + \frac{s}{2} \left[\alpha D_3^n f_3^n - D_2^n f_2^n \right], \quad (\text{A4})$$

and for the next to last point,

$$f_M^{n+1} = f_M^n + \Delta t \left(\frac{a_M^n f_M^n + a_{M-1}^n f_{M-1}^n}{\Delta x_{M-1} + \Delta x_M} \right) + \frac{s}{2} \rho \left[-D_M^n f_M^n + D_{M-1}^n f_{M-1}^n \right], \quad (\text{A5})$$

where $M = N - 1$, and N is the total number of points in energy space. For the third point (x_3), the only change needed to be made is to set the coefficient ρ in Equation (A1) to $\rho = q$.

Because Equations (A4) and (A5) employ only two boundary points instead of three as any other $k \neq 2, M$, it is not possible to make the scheme conserve particle number *and* energy simultaneously for these two bins. We need two parameters to conserve these integrals, while we have only one parameter available in Equations (A4) and (A5) (i.e., the ratio α/ρ). Physically, by bouncing particles scattering into the first bin back to the second and third bins ($f_1(t) \equiv 0$ at all times), we conserve the number of particles, but *change* the energy of these particles to make them stay inside this energy range (i.e., inside the region $x_2 \leq \gamma - 1 \leq x_{N-1}$). This process therefore does not conserve energy, and we must subtract this excess energy from the total energy change during each iteration. Practically, this is done by introducing a small correction to the electron energy exchange coefficient, which allows us to conserve energy up to double precision accuracy during the entire particle thermalization time.

Note that the mirror boundary conditions are perfectly physical and are applicable to any electron distribution function with large or small deviations from a Maxwellian. Indeed, if there were a physically substantial flow through the low energy boundary, that would mean that there is either a source or sink of particles with $E \ll \Theta_e$, where Θ_e is the dimensionless electron temperature, $\Theta_e \equiv kT_e/m_e c^2$. While this situation is mathematically possible, it is not plausible physically (if there is an influx of cold electrons from outside into the system, one can always choose the low energy boundary such that it includes these electrons). On the high energy end, any electron acceleration mechanism can only accelerate electrons to some maximum energy (specific for this mechanism), after which electron cooling overcomes the heating. Therefore, if one chooses the high energy boundary much higher than this maximum energy, then there can be no flux through the boundary, since the electrons get ‘turned back’ to lower energies before they reach the boundary.

The ultimate test of the given scheme is to see how close the equilibrium distribution function approaches a Maxwellian (when one includes only the lepton-lepton FP part of the full lepton Boltzmann equation). We have run a number of tests (described in the next few sections) and find excellent agreement between the equilibrium distribution and a Maxwellian (with a relative deviation of less than 2%).

A.2 Numerical Stability Of The Scheme

Equation (A1) is a non-linear integro-differential equation, for which strictly speaking, the usual Von Neumann analysis should not be used to test its stability. Fortunately, the fact that the FP coefficients are integrals over the distribution function makes the stability analysis essentially linear. Conducting the stability analysis of our scheme as if $a(E, t)$ and $D(E, t)$ are fixed functions, or at most, slowly varying functions compared to $f(E, t)$, and using the usual Von-Neuman approach (e.g., Press et al. 1986), we arrive at the approximate stability criterion:

$$\max \left\{ \left(1 - \frac{D_k^n \Delta t}{(\Delta x_k)^2} \right)^2, \left(\frac{a_k \Delta t}{\Delta x_k} \right)^2 \right\} < 1. \quad (\text{A6})$$

Equation (A6) is a necessary condition for the scheme (Eq. A1) to be numerically stable. While this condition is only approximate, we find that by choosing a time step roughly equal to or smaller than that which satisfies Equation (A6), our differencing scheme is always stable.

For applications where ‘exact’ energy conservation is not an issue (e.g., in systems with a low optical depth and a high compactness, such that the energy is radiated efficiently from the system), we were able to develop a half implicit-half explicit scheme that is much faster than the explicit scheme (see the next section).

A.3 The Numerical Procedure

We follow the procedure outlined in §A.1 above, except that we here include the additional terms corresponding to Compton interactions and proton heating. The particle distributions are evolved more often than the photon distribution, i.e., the photon distribution is kept fixed during a time $\Delta t_M = M\Delta t$ while the particles proceed through their evolution a number M ($\gg 1$) of Δt steps. This approach is necessary because otherwise in each time advancement, one needs to re-evaluate the photon annihilation cross section and the Compton scattering matrix, among others. This increases the computation time considerably. The value of Δt is dictated by the stability criterion given in Equation (A6). It turns out that this condition is much stricter than any other criterion for Δt based, e.g., on the requirement that distribution functions change very little during one time advancement (i.e. $|\Delta f(E)| \ll |f(E)|$). The latter should be used for determining the time step when evolving the photon distribution since there is no numerical instability problem analogous to Equation (46). We are therefore justified in using $\Delta t_M \gg \Delta t$.

The computation time depends considerably on whether one uses explicit or implicit schemes and on the Thomson optical depth of the system. For a Thomson optical depth $\tau_T \sim 1$, the explicit scheme takes a few days on a Pentium PC running Linux (for 70 bins in the electron energy space and 70 bins for photons), whereas an implicit scheme takes from 6 hours to a day. Obviously, such a long computing time makes it difficult to use the described methods in practice, for example to fit observations.

For most of the applications, however, a time-independent code should suffice. We have been able to write and use such a code successfully. Using the approximate solution of the full electron equation given by Equation (50), and assuming that the positron distribution is same as that of the electrons, we were able to reduce computing time to 2 – 5 minutes. In essence, the code is not any slower than a corresponding code that assumes that particles are thermal and takes into account the same interactions and follows radiation transport in the same manner. Thus, the time-independent code is highly efficient and might easily be used in X-ray fitting packages, such as XSPEC. This code and some results are to be published elsewhere (the results presented in the current paper were obtained using the full time-dependent implicit code). The authors can provide their code for use by anybody who feels a need to use exact particle distributions.

To verify that our code was correctly resolving the particle distribution in energy space, we also varied the number of energy points. A comparison of our results from a test with 100 energy bins (for both electrons and photons) with those from a simulation with 70, showed that the relative differences in the distribution, spectrum, temperature and the number of positrons were $\lesssim 1\%$.

A.4 Large Angle Scatterings

As already mentioned in §3, it has been known since the early work of Chandrasekhar and Landau that large angle scattering events are not important for Coulomb interactions in a gas, since the rate of energy exchange due to these is much smaller than that due to small angle collisions. This point is worth discussing further here, since it appears to be the basis for the difference between our approach and that of Dermer & Liang 1989. Large angle scatterings correspond to small impact parameters. We can estimate the latter for large angle scatterings r_l by writing

$$\frac{e^2}{r_l} \gtrsim |\Delta E| m_e c^2 \quad (A7)$$

(recalling that $E \equiv \gamma - 1$ is dimensionless). The cross section is then $\sigma_l(\Delta E) \lesssim \pi r_l^2$, and the energy exchange rate is

$$a_l(E) \sim \sigma_l(\Delta E) |\Delta E| n_e \beta c \lesssim \pi \frac{e^4}{m_e^2 c^4} n_e c \beta / |\Delta E|. \quad (A8)$$

Let us consider the high energy portion of the electron distribution, i.e., $E \gg \Theta$. Large angle scatterings correspond to a large change in the electron energy $\Delta E \sim E$ (Equation [14]). Therefore, we can put $\Delta E = E$ in the above equation, and re-write it as

$$a_l(E) \sim \frac{3}{8} \frac{1}{t_T} \frac{\beta}{\gamma - 1}. \quad (A9)$$

Equation (30) can be used to estimate the small angle energy exchange rate

$$a_s(E) \sim 3/2 \frac{\ln \Lambda}{t_T} \frac{1}{\beta \langle \gamma \rangle}, \quad (A10)$$

where $\langle \gamma \rangle$ is the average thermal γ -factor. The ratio of the large angle energy exchange rate to that of small angle scatterings is thus

$$\frac{a_l(E)}{a_s(E)} \sim \frac{\beta^2 \langle \gamma \rangle}{\gamma - 1} \frac{1}{4 \ln \Lambda} \ll 1, \quad (A11)$$

as long as $\ln \Lambda \gg 1$. Let us now assume $E \ll \Theta$. In this case we should use the average thermal β and γ in Equation (A9), since the energy exchange can be as large as $\sim \Theta$, and β in equation (A8) is really the relative velocity of the two colliding particles, which is of the same order as the thermal velocity. The ratio of the scattering rates becomes

$$\frac{a_l(E)}{a_s(E)} \sim \frac{\langle \beta \rangle^2 \gamma}{\langle \gamma \rangle - 1} \frac{1}{4 \ln \Lambda} < \frac{1}{4 \ln \Lambda} \ll 1 \quad (A12)$$

A similar estimate holds for energies $E \sim \langle E \rangle$, except for the narrow region where the small angle energy-exchange coefficient goes to zero (Fig. [3]).

Therefore, it is evident that one may neglect the large angle scatterings in the full kinetic equation that describes Coulomb collisions. Moreover, we argue that it is even necessary to do so in the calculation of the FP coefficients, since otherwise the approximation made for small scattering angles becomes invalid for large angles and can lead to wrong conclusions. Physically, one cannot

decompose the electron distribution function in the original Boltzmann kinetic equation, since the large angle scatterings do not constitute a diffusion process. For example, the use of the diffusion coefficient as computed by Dermer & Liang (1989) can lead to a power-law electron distribution on the high energy end instead of a Maxwellian distribution, if other interactions, such as inverse Compton cooling are not important. The large angle scattering terms, which according to the above discussion should contribute very little, in fact start to dominate the diffusion coefficient. The energy exchange coefficient, on the other hand, is unaffected by the inclusion of these terms since (by coincidence) averaging over ϕ^* cancels out the large positive and negative ΔE in Equation (14).

Figure 1

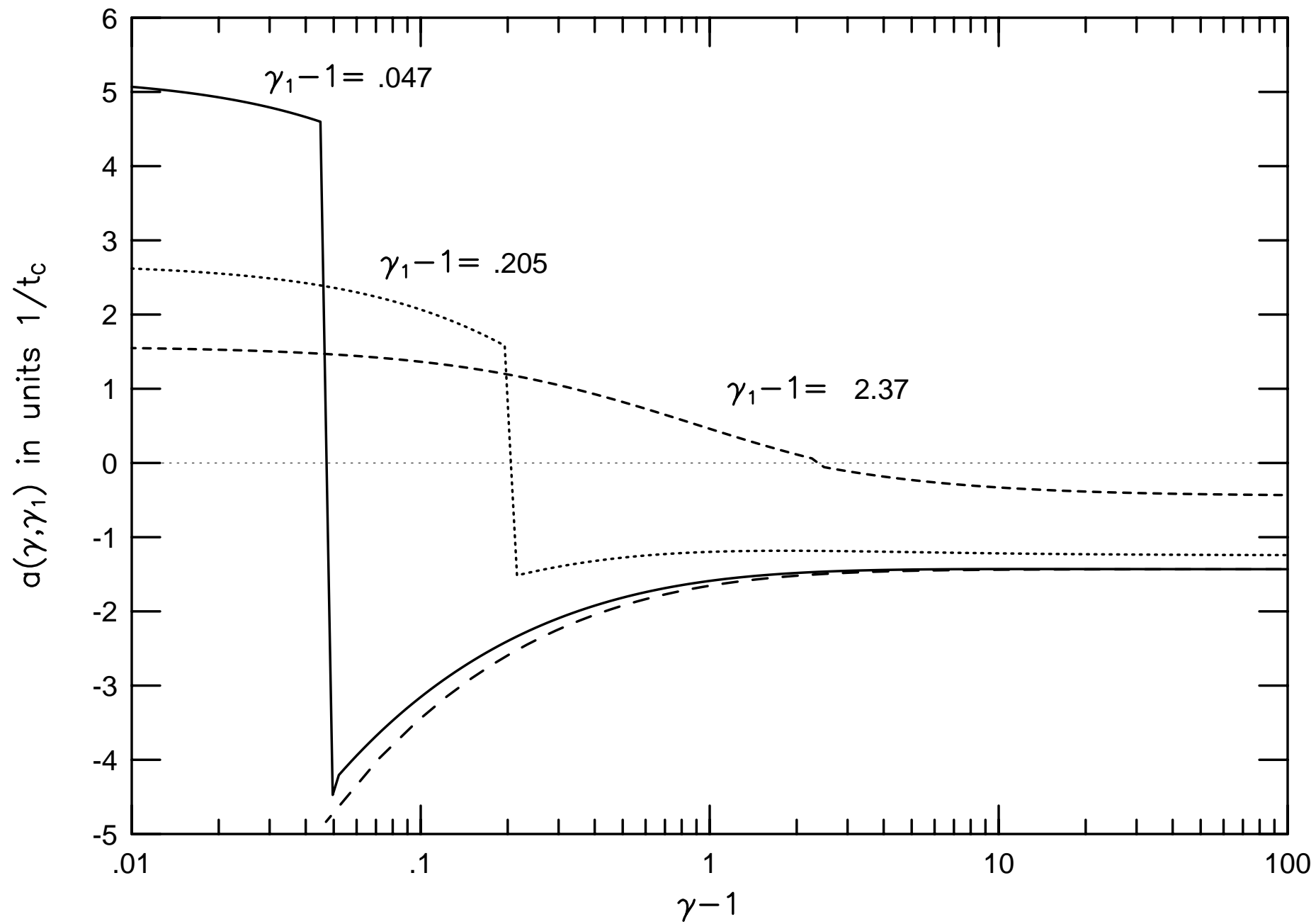


Figure 2

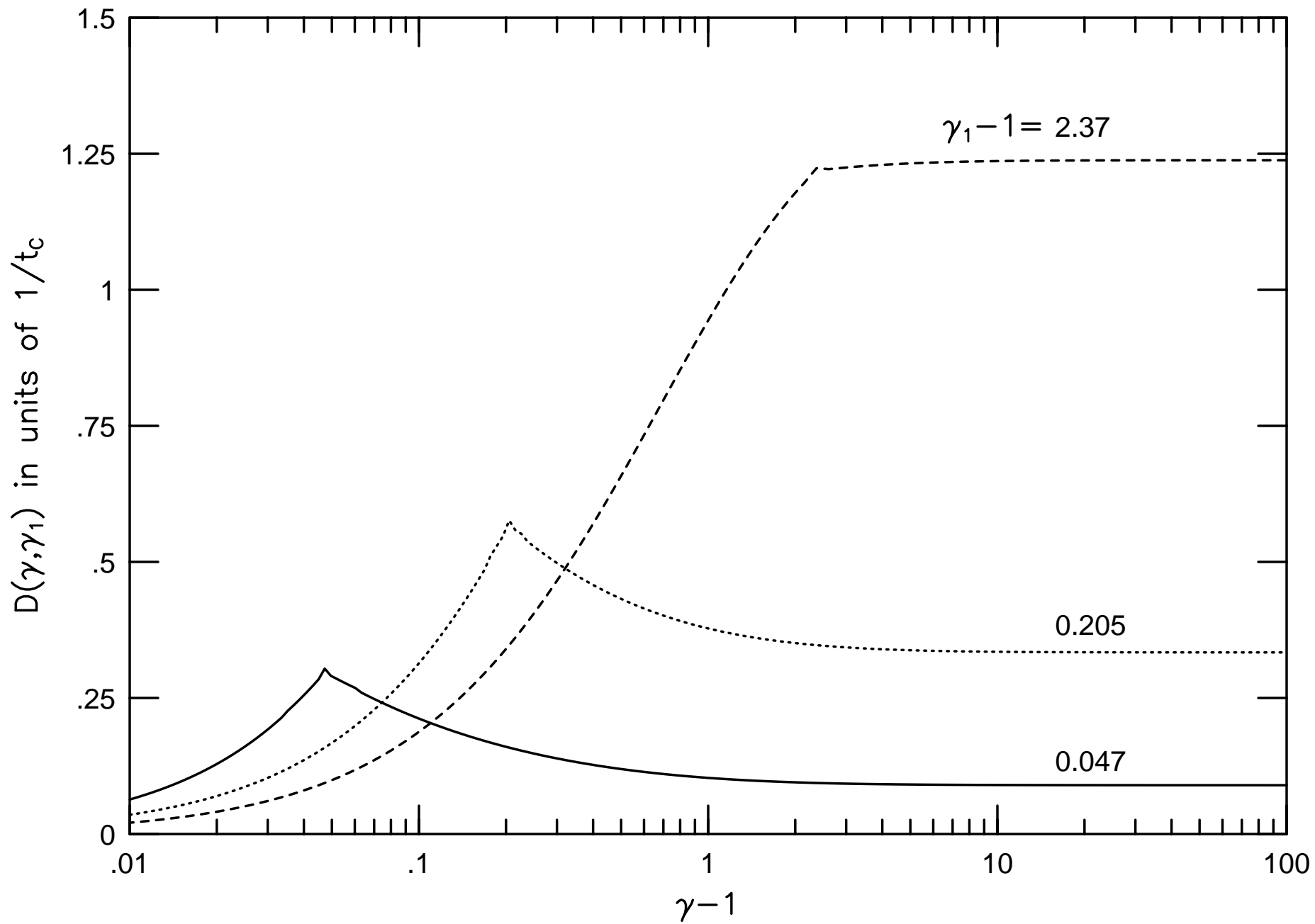


Figure 3

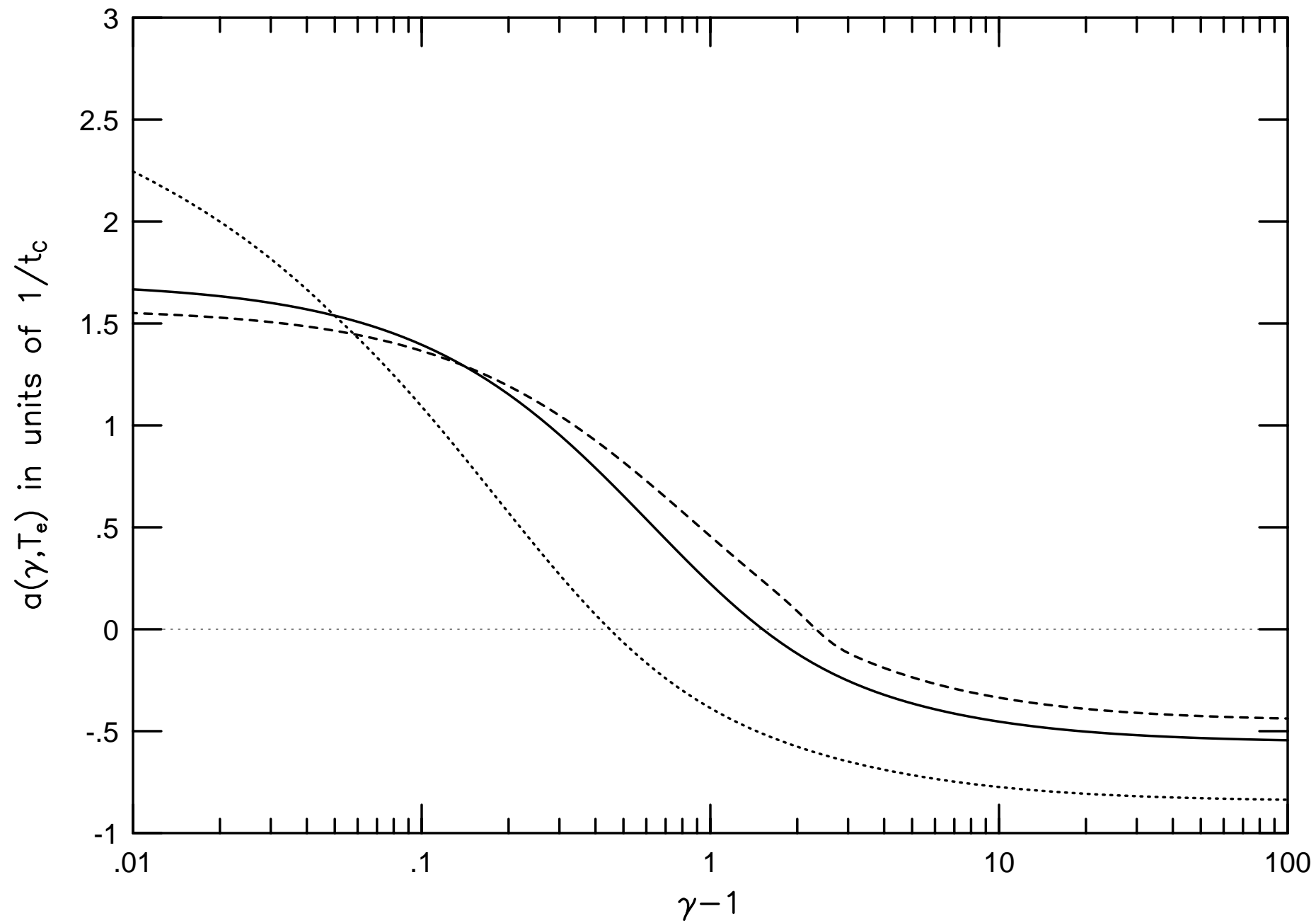


Figure 4

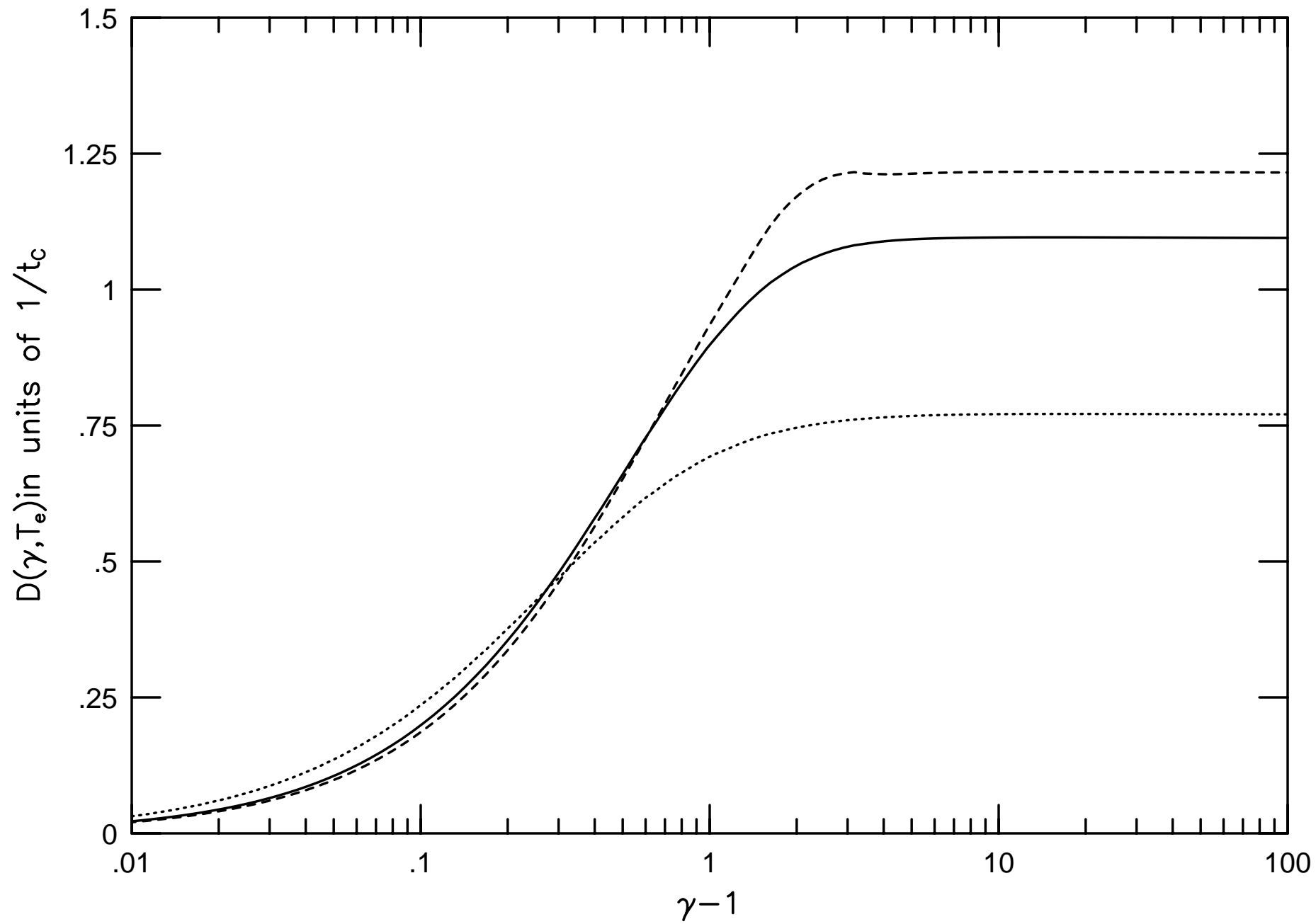


Figure 5

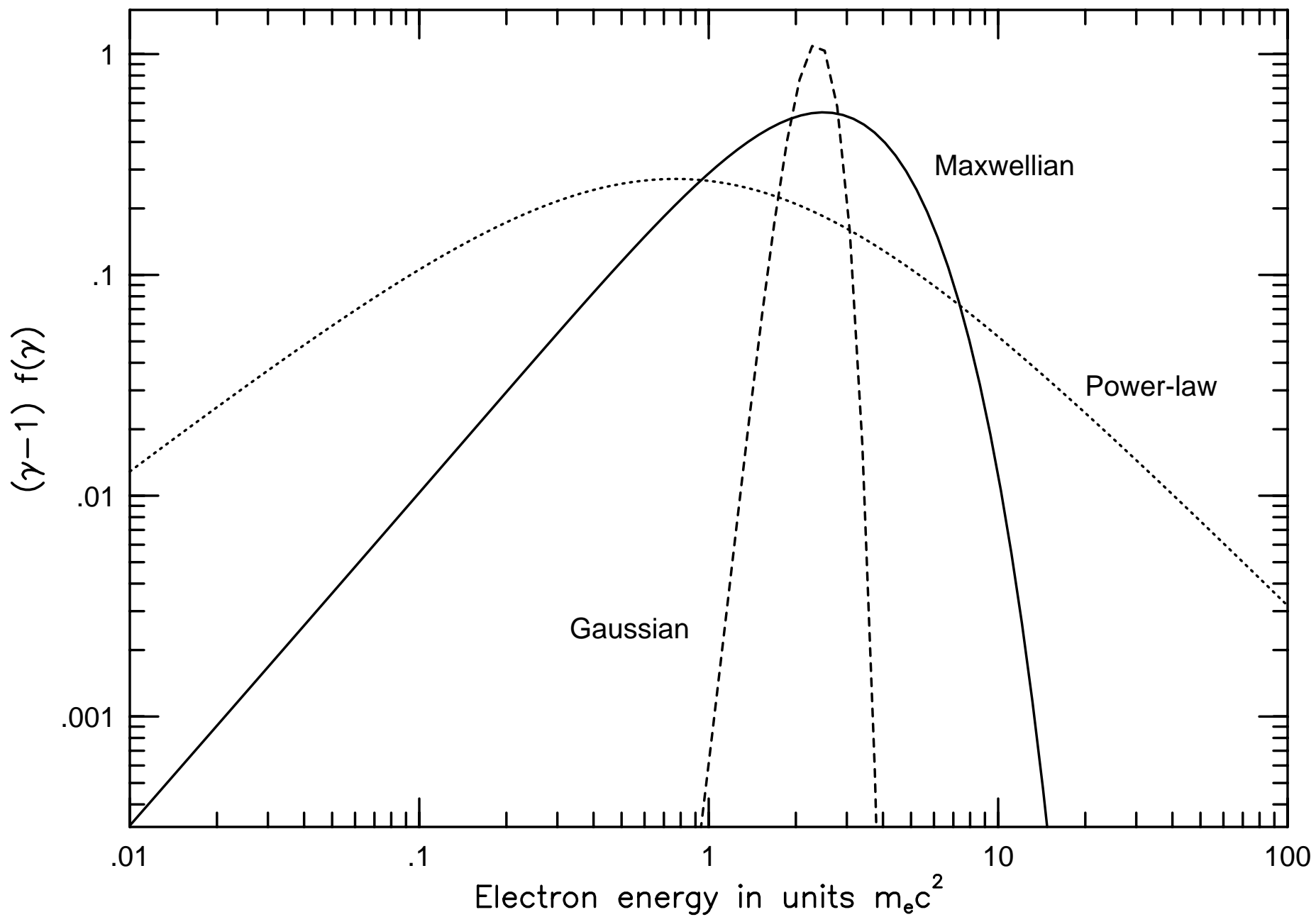


Figure 6

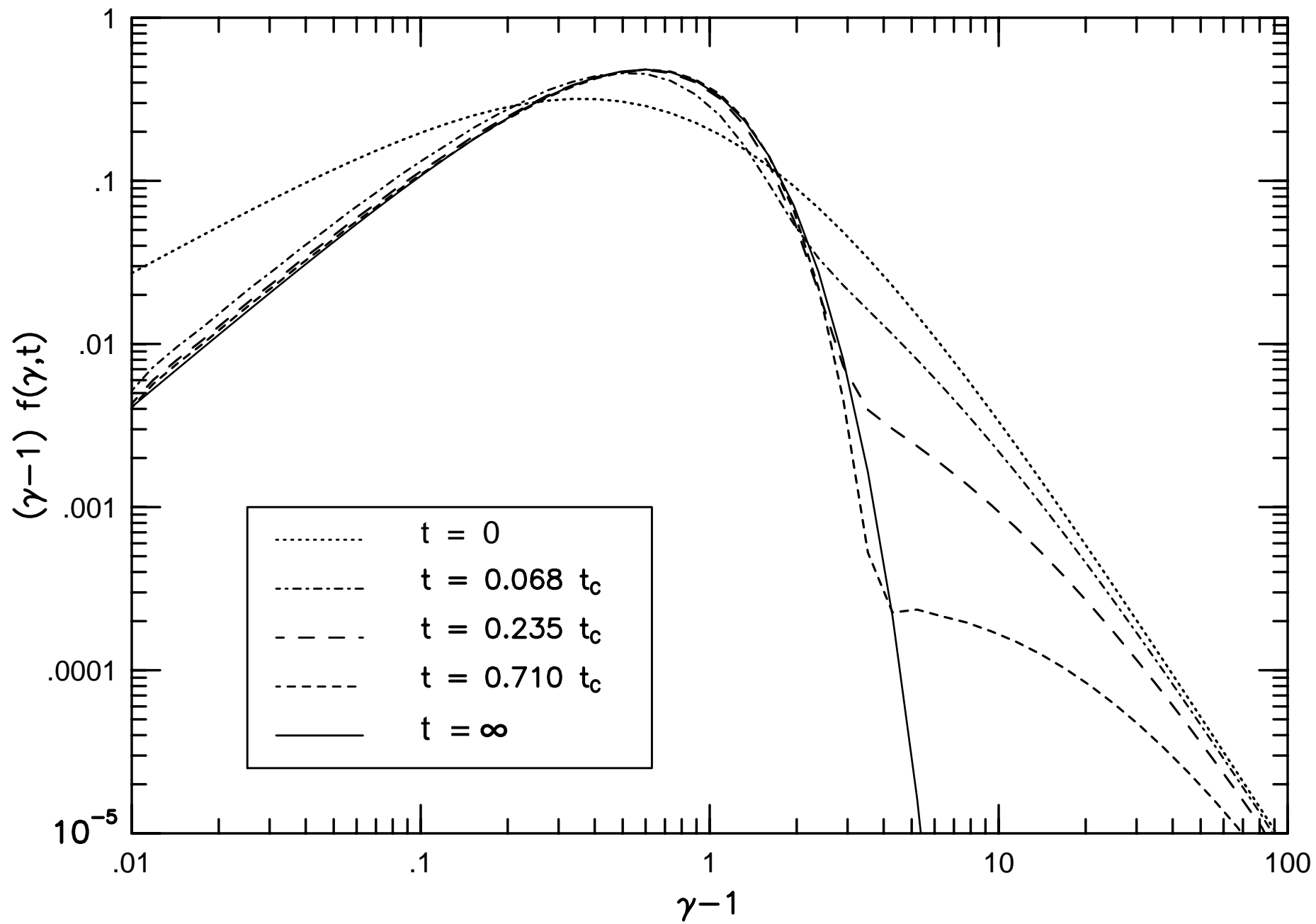


Figure 7

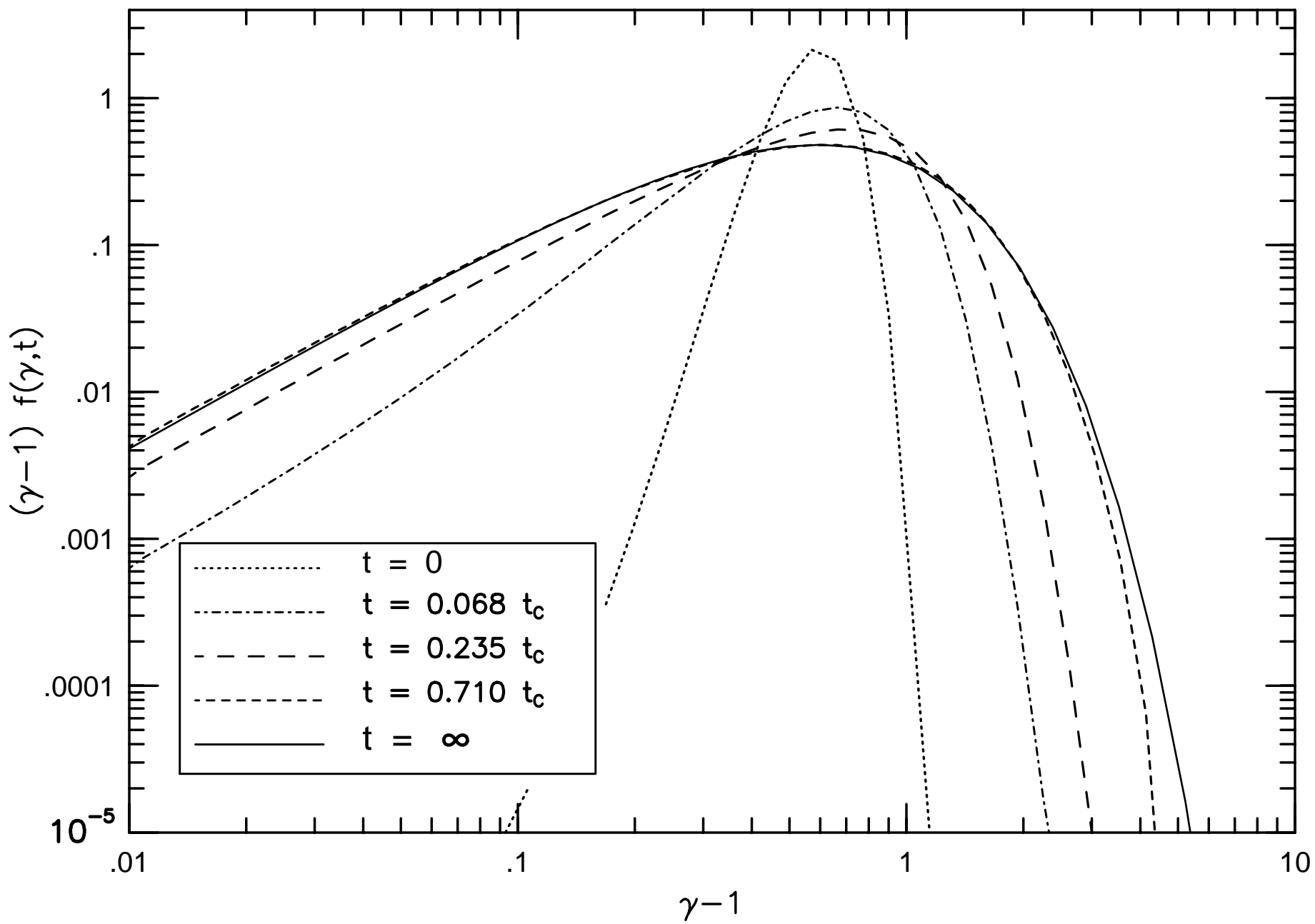


Figure 8

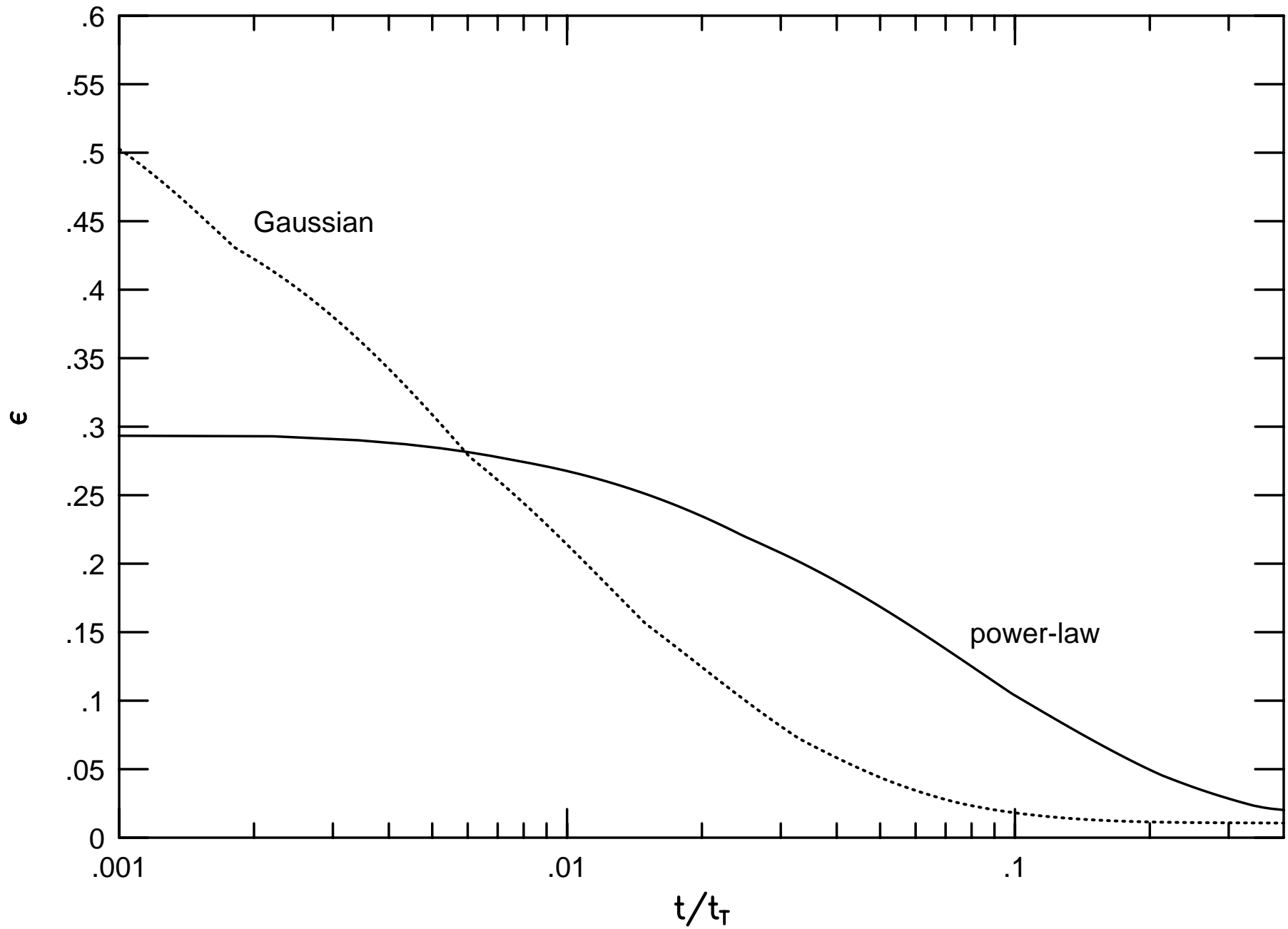


Figure 9

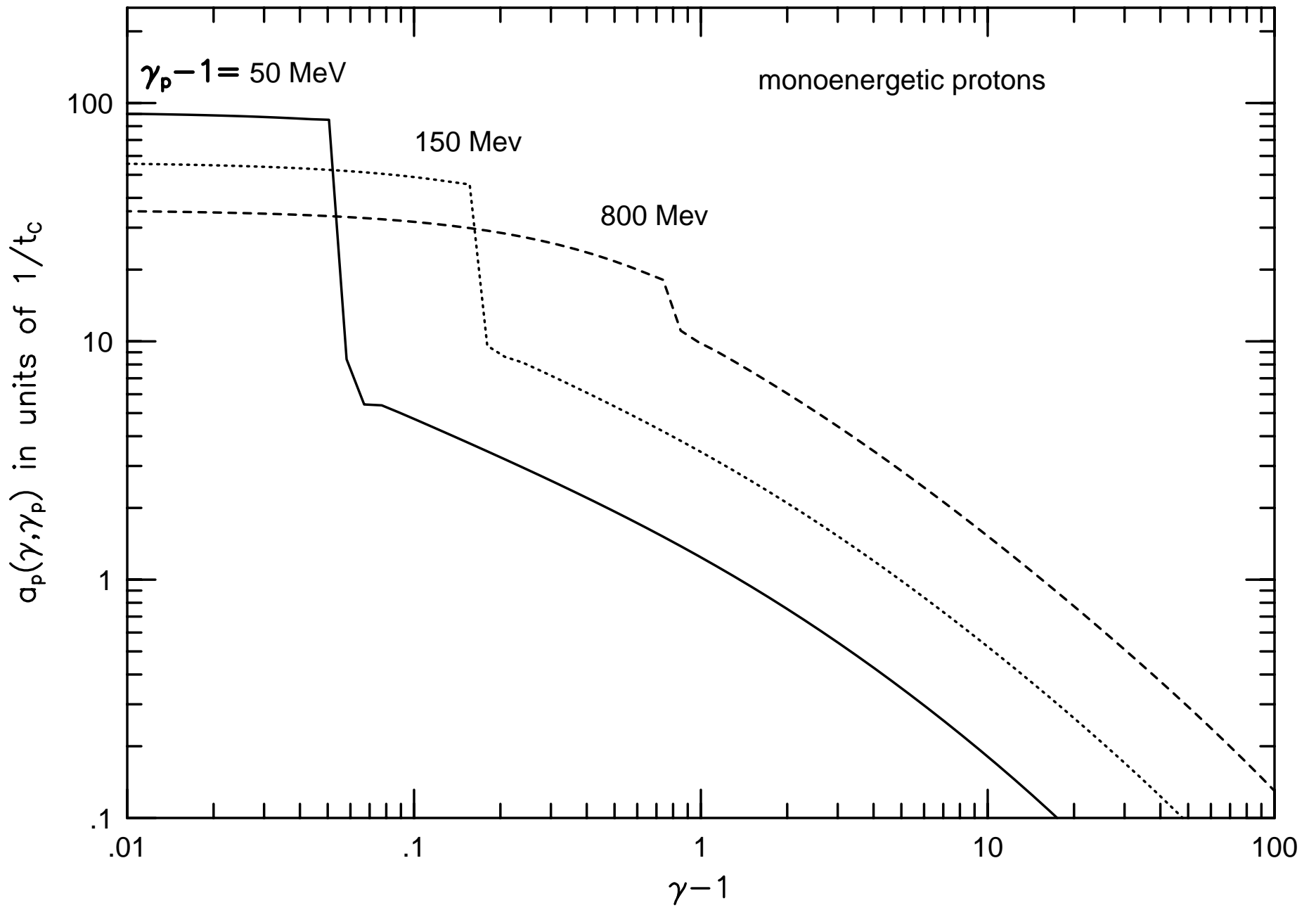


Figure 10

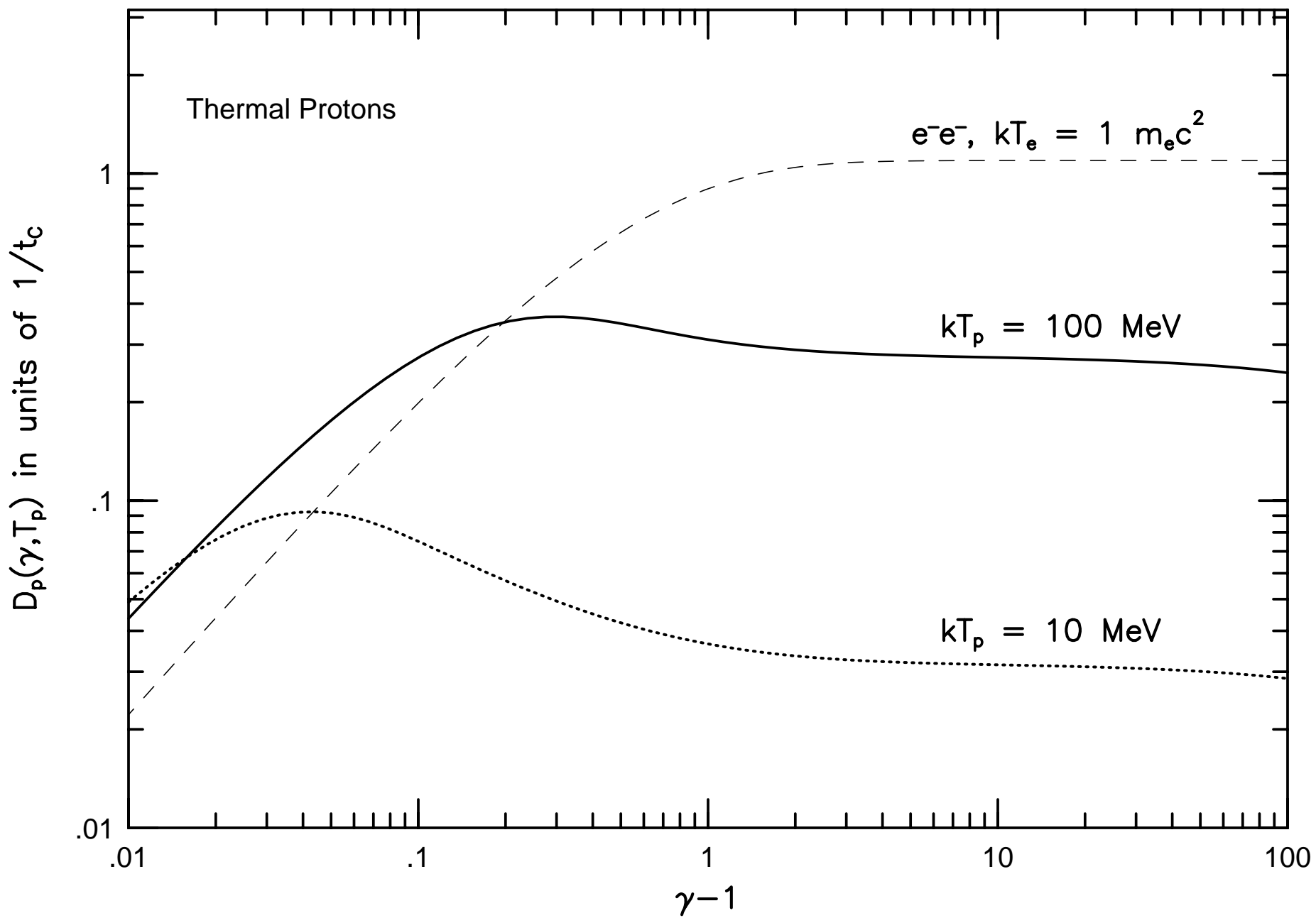


Figure 11a

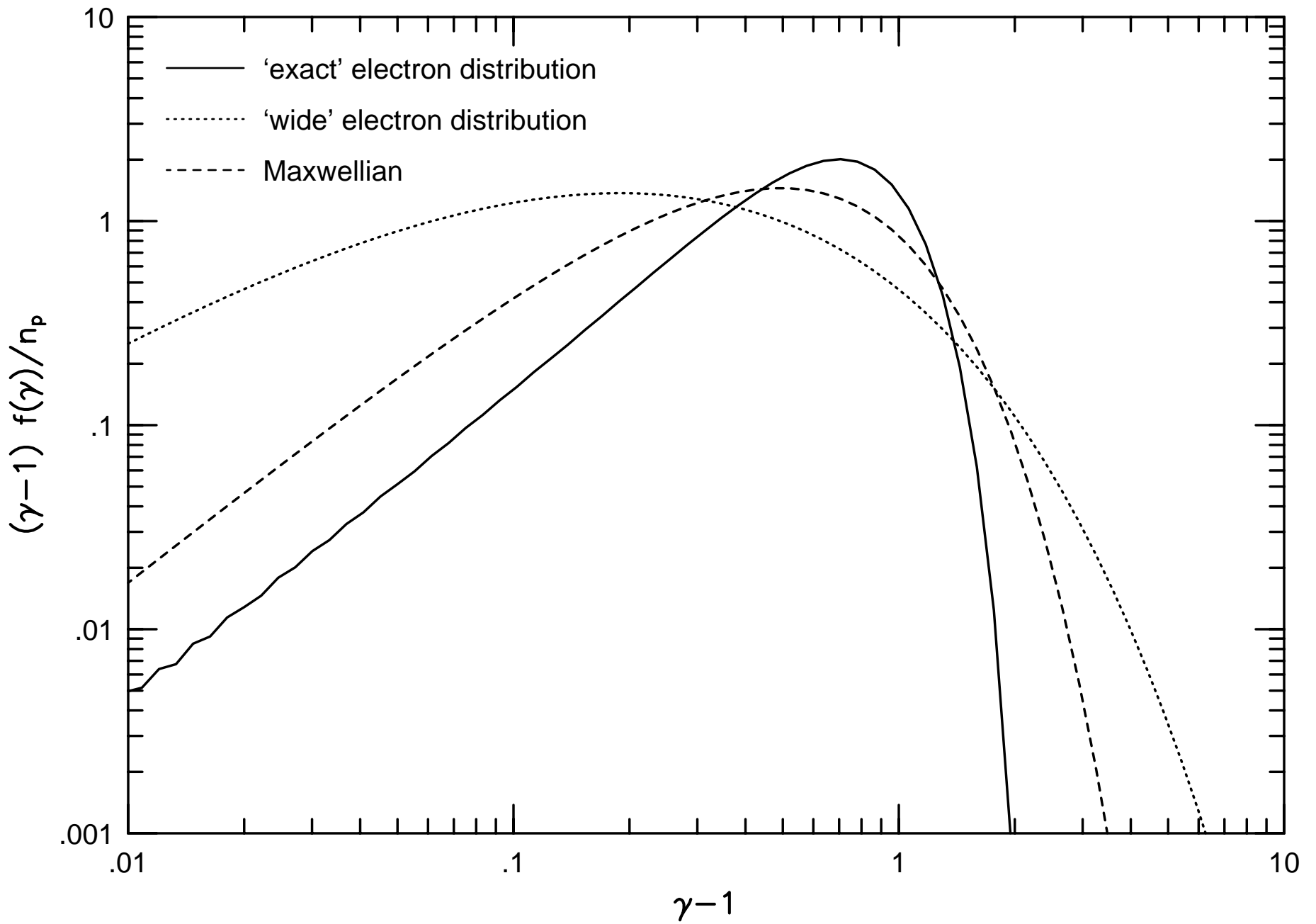


Figure 11b

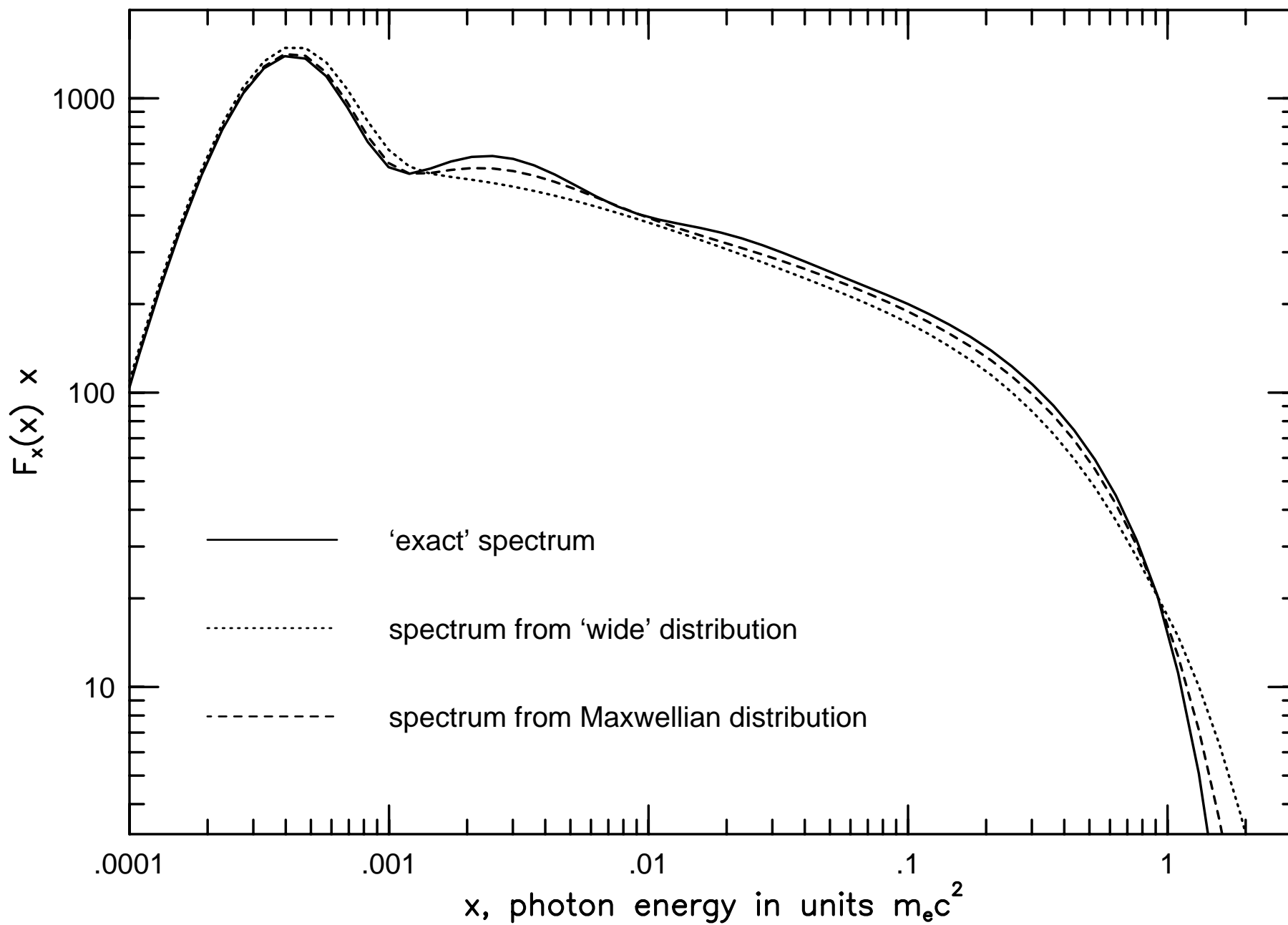


Figure 12a

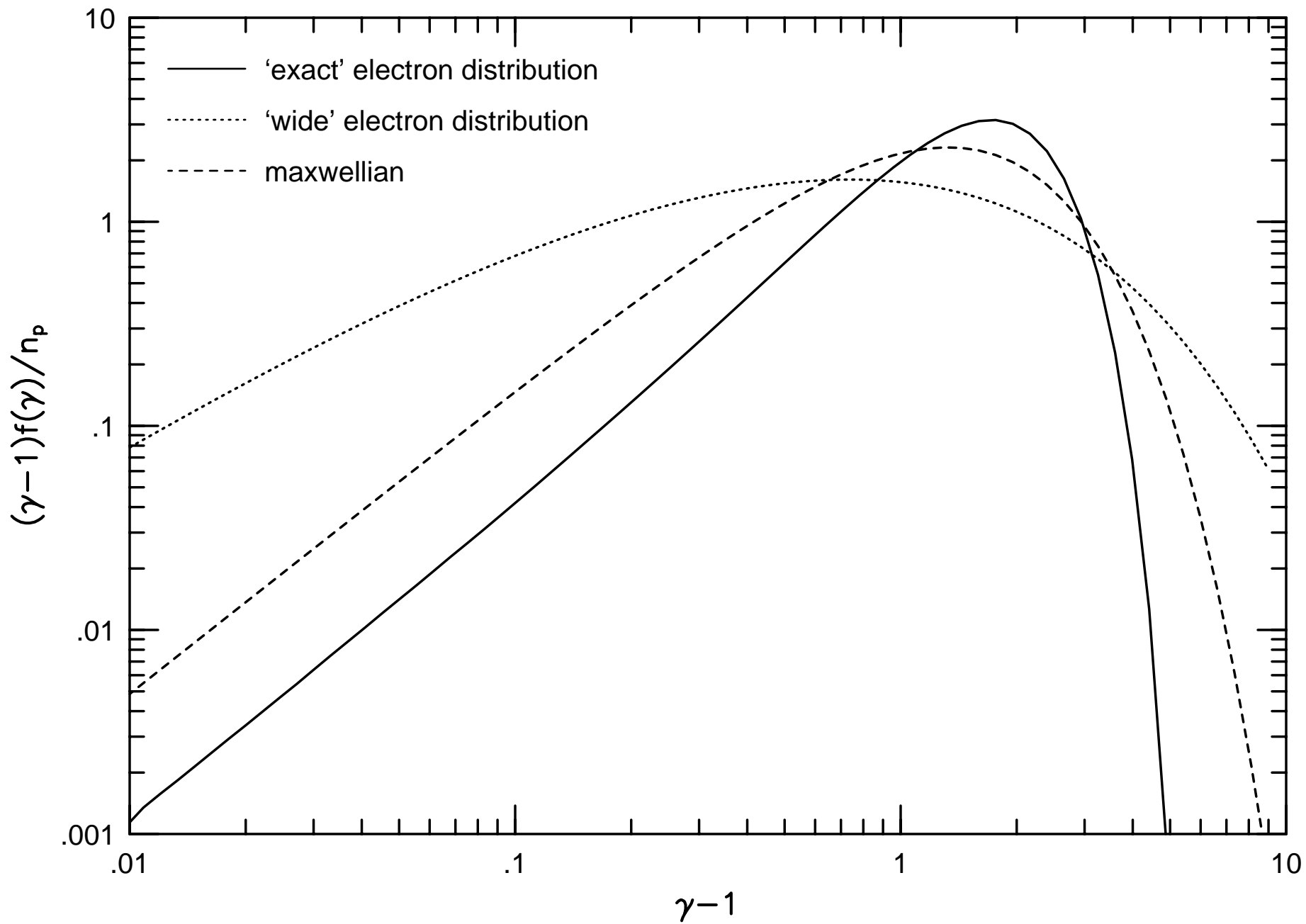


Figure 12b

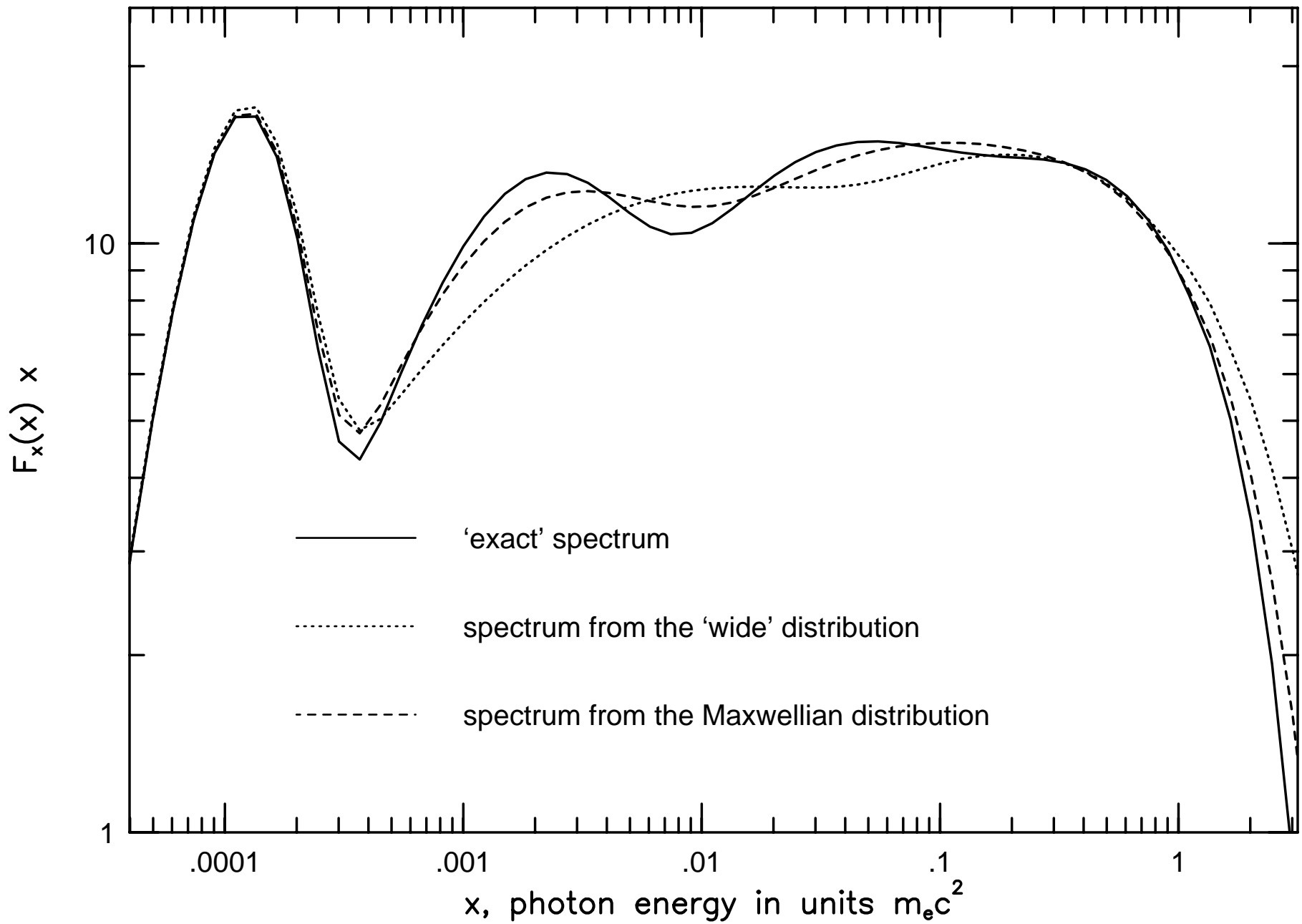


Figure 13a

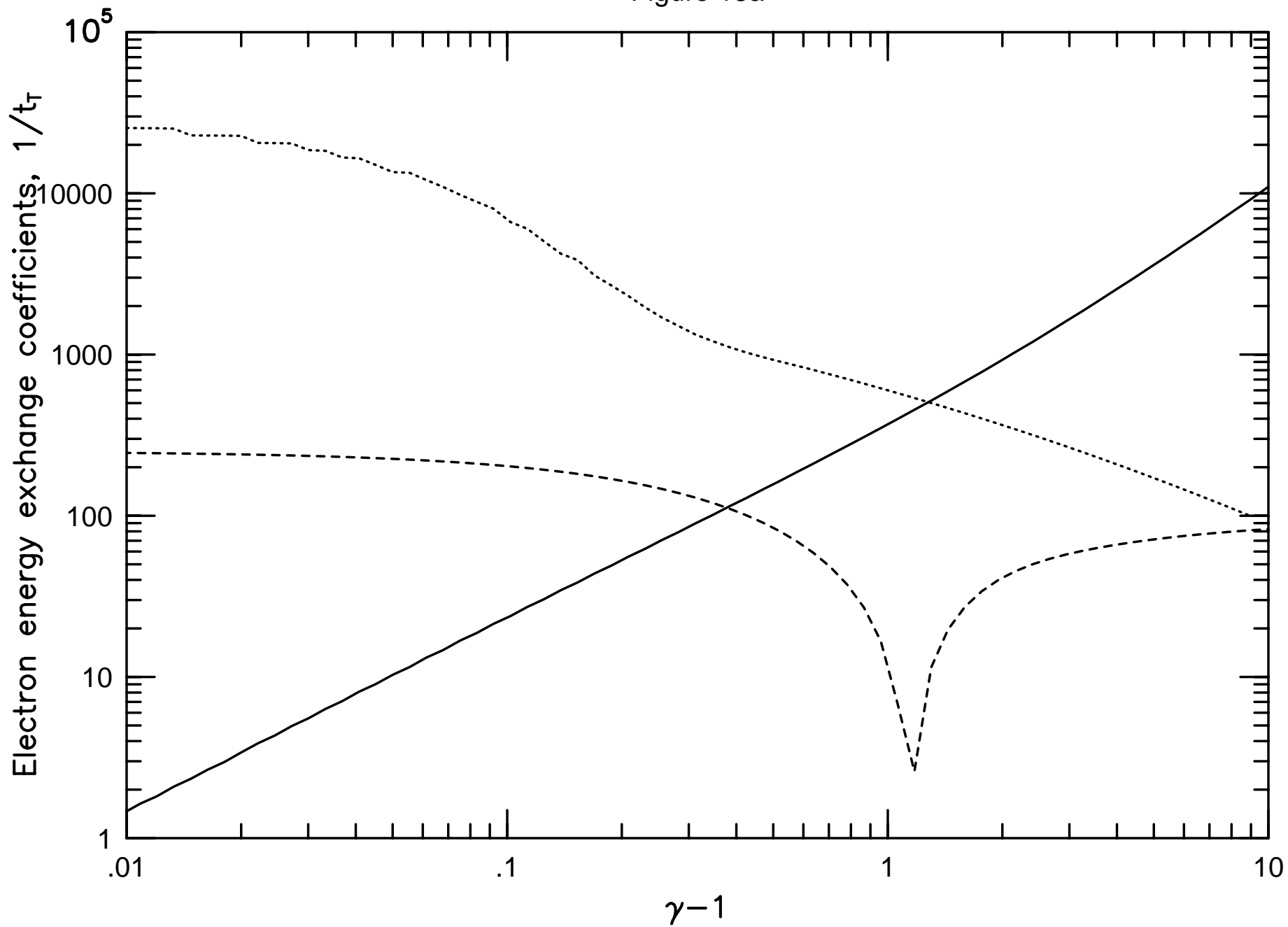


Figure 13b

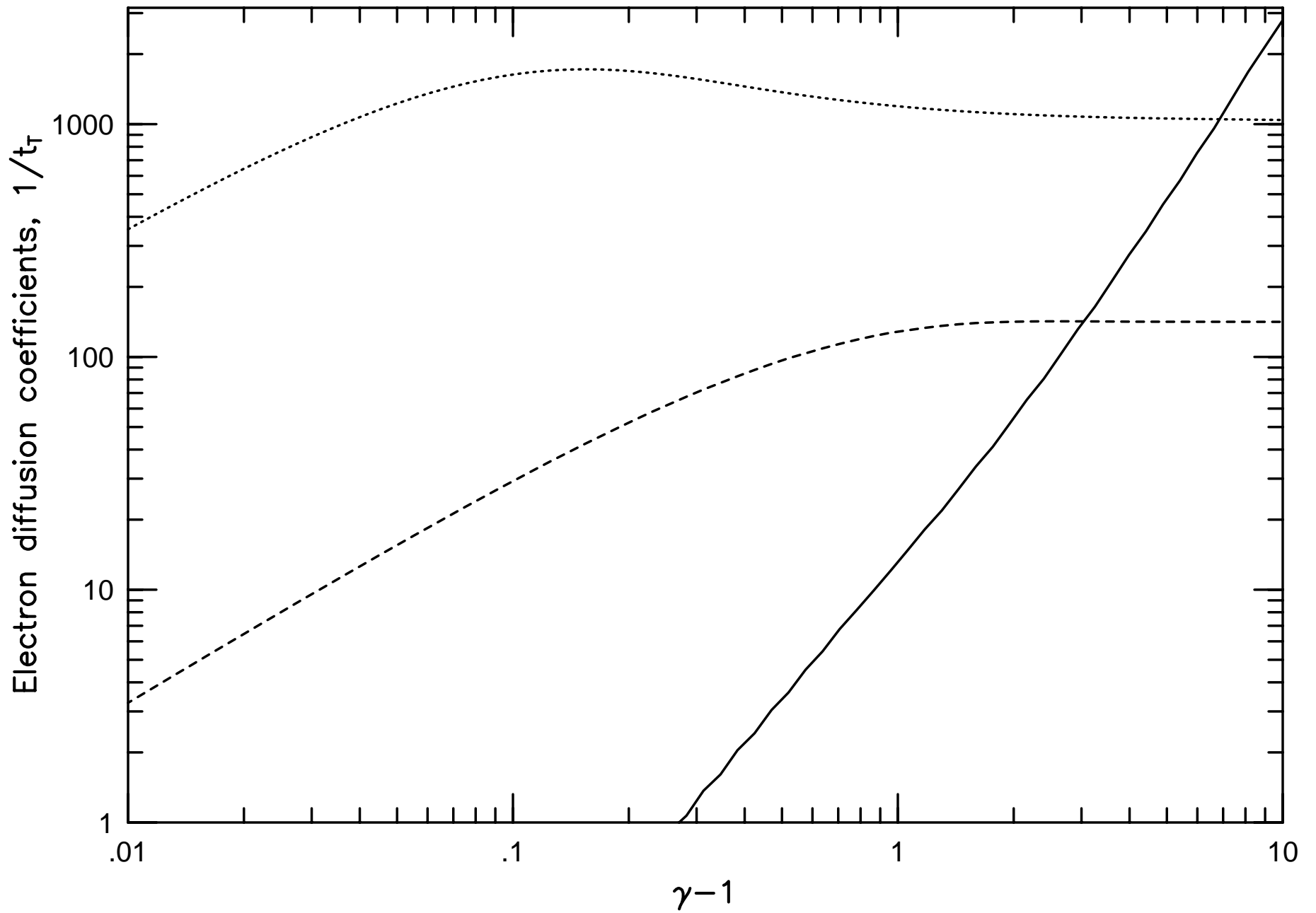


Figure 14

